APPLICATIONS OF OPTICAL METHODS TO SURFACE MICROTOPOGRAPHY

Dissertation presented for the degree of

Master of Science

in the

University of London

by

R.V.Williams

June 1956

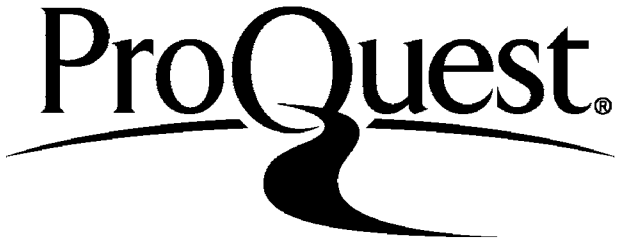

ABSTRACT

Several optical methods for the examination of the microtopography of surfaces are discussed. They divide themselves naturally into two groups; those which give quantitative information about the surface and those which give only qualitative information. There is a bias towards the first part.

With reference to part A, the quantitative methods, the techniques discussed are, Fizeau and F.E.C.O. multiple beam interference fringes, both in reflection and in transmission, two beam interference microscopes, the profile , and the shadow casting techniques. A separate chapter deals with the properties of the reflecting coatings used in some of the above methods. Part B is concerned with the application of phase contrast methods to the study of surfaces, that is in the vertical illumination microscope.

CONTENTS

Introduction

The microscopical techniques disscussed in this dissertation are those which reveal surface heights and depths. Most of them in fact not only show the microtopography, but measure it as well. In other words methods are dicussed in which differences in surface level are changed into amplitude variations in the image plane of the microscope. The dissertation divides itself naturally into two parts, A, methods which give quantitative information about the surface, and, B, methods which give only qualitative information. No apology is given for the bias towards part A, as the majority of the methods discussed there have been developed in the laboratory in which the author works.

With particular reference to Part A, the various methods are each applicable to different conditions of observation. Fizeau multiple beam fringes, which give all the advantages of multiple beam interferometry to the study of surfaces, can resolve in depth down to about 50A. and in extension to about $\cdot 6\mu$. However there is also an upper limit, a few wavelengths, to the depth of structure which can be viewed using Fizeau fringes. F.E.C.O. have a rather greater lateral resolution, since the fringe dispersion is independant of wedge angle, and whereas Fizeau gives a general contour map of the surface, F.E.C.O. are more suitable for precise measurements. However these fringes require rather more interpretation to give a picture of the surface.

To cope with rougher structures, the surface profile technique was developed. This method can just resolve a cube

of side $\lambda/2$. Here the surface can be viewed and measured at the same time, but it is similar to F.E.C.O. in that it plots the cross-section of a line drawn on the surface. Lastly, to deal with really rough surfaces, the optical shadow-casting method, discussed in Section II, can be usad.

Part B deals mainly with the application af phase-microscopy to surface studies. It is an useful tool on the surfaces which can be viewed in this way, which are, in general, those which cah be examined by Fizeau and F.E.C.O. fringes. It is complementary to these techniques in that it gives a general picture of the surface "which looks like" the actual Microtopography.

CHAPTER I.

Transmission Fizeau Fringes

This chapter describes a simple, but elegant interference device which is used for the accurate measurement of surface topographical features. It is a refinement of the well known Fizeau interfereometer, so widely used for the optical working of glass and metal surfaces, and for many other metrological purposes. The interfereometer as commonly used for studying figure will now be described.

Two Beam Fizeau Fringes.

It is a matter of common experience that the colours formed in a thin air or oil film disappear as the film thickness increases. The cause of this can easily be seen on examining the optics of the formation of the thin film interference colours commonly seen (e.g. oil films in puddles).

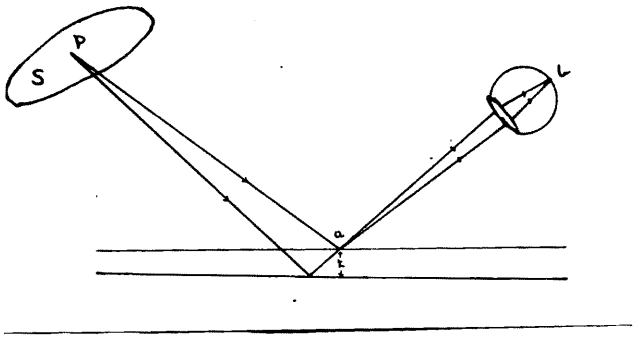

Fig. 1

The two coherent rays shown in the diagram originate from the same atom P in the extended source S and each atom in S sends out such rays. We consider only the case of interference effects localized in the front surface of the film, so the two interfering coherent rays are drawn meeting (a) in the film, and (b) at the retina of the eye. The state of interference at (a) is reproduced at (b). The colours in the film are governed by the well known formula

$$n\lambda = 2\mu t \cos\theta$$

where n is the order of interference, t the film thickness and θ the angle of incidence.

$$\text{So } dn\lambda = (-)\, 2\mu t \sin\theta\, d\theta$$

Now since the source is extended, θ will vary, tending to confuse the interference pattern at the film. For small values of t, the effects of varying θ are small and, provided t (and the entrance pupil of the viewing system) are small enough, we will have a relatively clear interference pattern in the film. But it can be easily seen that, for the given range of θ values admitted by the viewing system, as t increases further, the range of order values at any one point on the film will increase until no interference pattern is left.

FIZEAU in 1862 proposed a system where the incident beam

is highly collimated. The result is that much larger values of t can be tolerated. In the apparatus shown in Fig.2 a monochromatic source is condensed on to the small aperture A. The wavefront diverging from A is collimated by the lens D and falls on to the air film formed between the plates PC & QC.

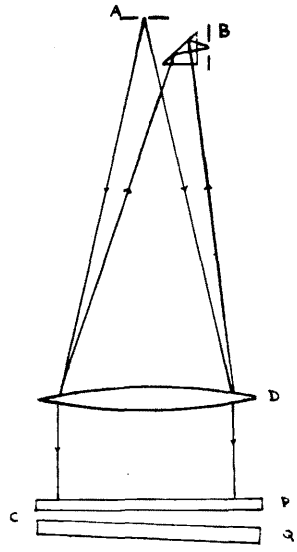

Fig. 2

The reflected light is focussed onto the aperture at B by passing through D again and by total internal reflection in the right angled prism R. If the eye is placed at B it will see the two beam interference fringes localized in the film between PC and QC. Now since, $n\lambda = 2\mu t \cos\theta$

gives the position of the fringe maxima and since θ is constant the pattern will be a contour map of the optical thickness (μt) of the plates, with the maxima a thickness $\lambda/2$ apart. So if the UPPER plate is an optical flat, we will see the topography of the upper surface of C$_2$. This method was first used for the study of surface toporgaphy by LAURENT (1883), and by SIEGBAHN (1933) for studying crystal surfaces in particular. It is widely used in optical workshops today as a routine test of figure but is limited by the broadness of the fringe pattern.

The Use of Highly Reflecting Surfaces in Interferometry.

The interference fringes obtained in the Fizeau system described above are formed by two beam interference, and so the resultant intensity is,

$$I = I_0 \cos^2(\phi/2) \qquad (1)$$

$$\text{in which} \quad \phi = \frac{2\pi}{\lambda}(2\mu t \cos\theta) \qquad (2)$$

The reflected two beam fringe system has an even worse fringe definition, given by

$$I = I_1 + I_2 + 2 a_1 a_2 \cos\phi$$

Here I_1 and I_2, a_1 and a_2 are the intensities and amplitudes of the interfering rays. For the reflection case $I_1 \simeq I_2$ and so (2) reduces to (1). But in transmission

I_1 and I_2 are not even of the same order of magnitude, with the result that the fringe pattern has the intensity distribution shown in Fig. 3.

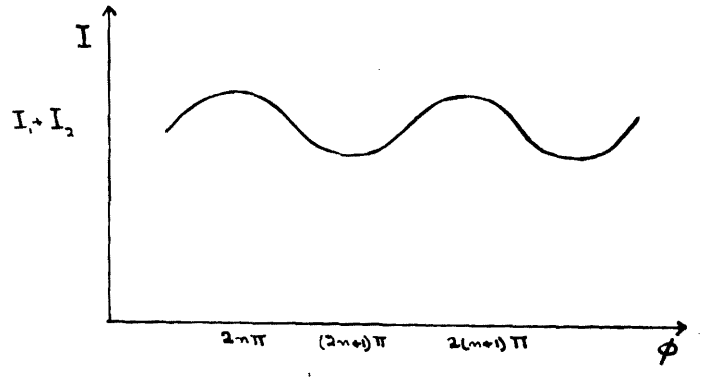

Fig. 3

Fig. 4 is an example of a two beam transmission interference pattern.

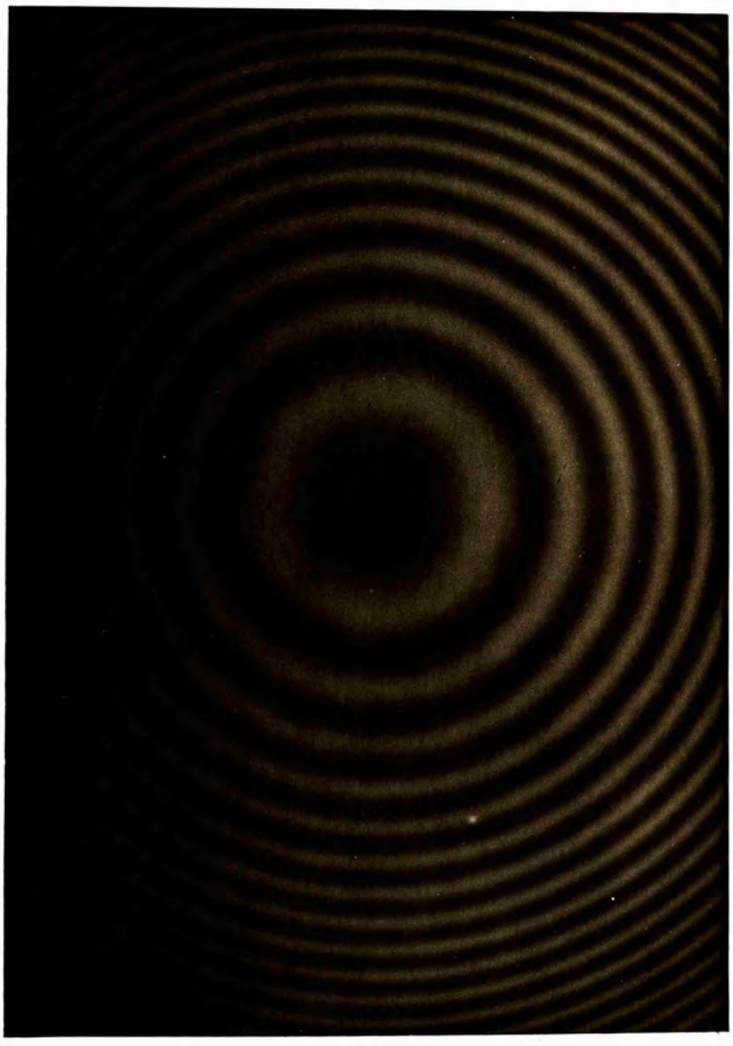

Fig 4. Two-Beam Newton's Rings Pattern.

Whilst two beam fringes are useful for the optical working of surfaces and for general metrological purposes, they are not so suitable for the precise measurement of surface topographical features, as is evident from Fig. 4. The flat topped nature of the fringes is unfavourable for the determination of fringe positions. Settings on a maxiumum cannot be made to better than $\frac{1}{20}$ of the distance between orders at the best, corresponding to an uncertainty of $\frac{\lambda}{40}$ in film thickness.

An important advance was made in 1893 by BOULOUCH, who pointed out that if the surfaces are semi-silvered, and so multiple reflections at the inteferometer surfaces become important, the fringe shape undergoes a remarkable change. FABRY and PEROT (1897) utilized his suggestion in their elegant inteferometer and credit is often wrongly assigned to them for the realization of the significant effect silvering has upon fringe width.

This effect is demonstrated by a study of Airy's expression for the transmitted intensity of an interferometer consisting of two, semi-silvered parallel plane plates, as

shown in Fig. 5.

An air film is considered, so refraction effects may be ignored in the calculations. When a collimated beam of monochromatic light falls upon the plates and the emerging beams are collected by a lens L_2 (see Fig. 6), we have, in the focal plane of L_2,

$$I = \frac{T^2}{(1-R)^2} \cdot \frac{1}{1 + \frac{4R}{(1-R)^2} \sin^2\left(\frac{S}{2}\right)} \qquad (3)$$

- See AIRY (1831)

This can be written,

$$I = I_{max.} \cdot \frac{1}{1 + F \sin^2\left(\frac{S}{2}\right)} \qquad (4)$$

- See TOLANSKY (1948)

Here I is the transmitted intensity, T and R the intensity reflection and transmission coefficients of the two interferometer surfaces (assumed identical), and

$S = 2 \times \frac{2\pi}{\lambda}$ (optical gap between interferometer plates for an angle of incidence, θ)

F is called the "coefficient de finesse" after Fabry. This formula assumes that an infinite number of beams is collected by L_2; this is approximately true for small angles θ .

The point of interest is the variation in the fringe

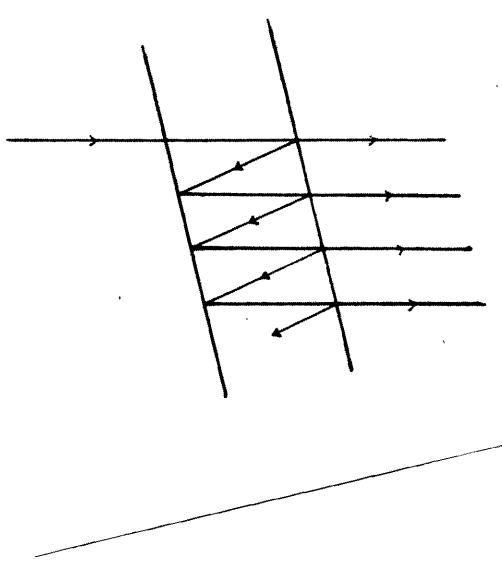

Fig. 5

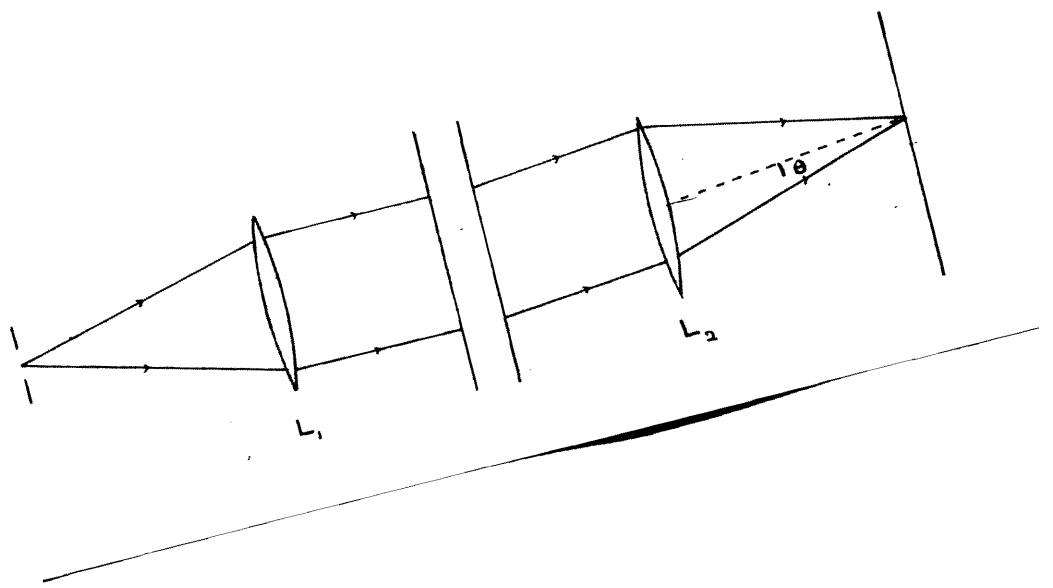

Fig. 6

width with the quantity F. It can be seen from (4) that, if F is large, as δ goes from $\delta = 2n\pi$ to $\delta = 2n\pi + d\delta$, I will fall rapidly from I_{max} to quite a small value, and stay there until δ reaches the region of $2(n+1)\pi$. The accompanying table shows that quite large values of F are found for values of R in the region •7 to 1.
This table is taken from TOLANSKY (1947).

R%	70	75	80	85	90	95
F	31.1	48	80	107	360	1520
I_{min}%	3.22	2.04	1.23	0.66	0.28	0.06

Fig. 7 shows the fringe shape for these different high values of R.

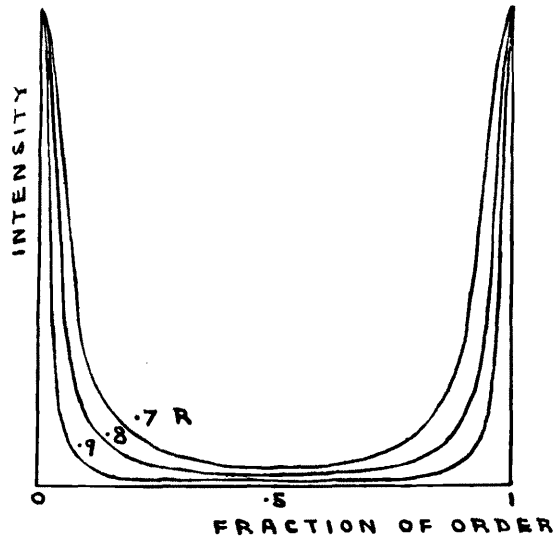

Fig.7

The bottom line in the table is the value of the minimum intensity as a fraction of the maximum. Evidently this type of fringe pattern is considerably more suitable for the precise determination of order displacements than the two beam $\cos^2$ distribution discussed above.

It was not until 1944 that the correct experimental conditions for using this type of intensity distribution in the Fizeau "equal thickness" set-up described above were discussed by TOLANSKY. He used it to obtain extremely sharp Newtons rings (1944, a) and with them was able to measure accurately the differential phase change on reflection of the two plane polarized components at non-normal incidence (TOLANSKY 1944, b). He then used these fringes, both in reflection and in transmission to contour a natural surface of quartz (TOLANSKY 1945, a) and cleavage surfaces of mica and selenite (TOLANSKY 1945, b). He showed that steps of the order of 30 Å.u., which is of the order of molecular dimensions, could be measured accurately, with simple apparatus, provided that certain simple experimental conditions were strictly adhered to.

Since then multiple-beam Fizeau fringes have been used, both in transmission and in reflection, for the study of many problems in surfaces micro-topography. They have been discussed by TOLANSKY (1946, c) and BROSSEL (1947). HOLDEN (1949) has discussed the reflection system in detail. The

following photographs show clearly how powerful a tool they are for the evaluation of the heights and angles associated with the microtopographical features of surfaces.

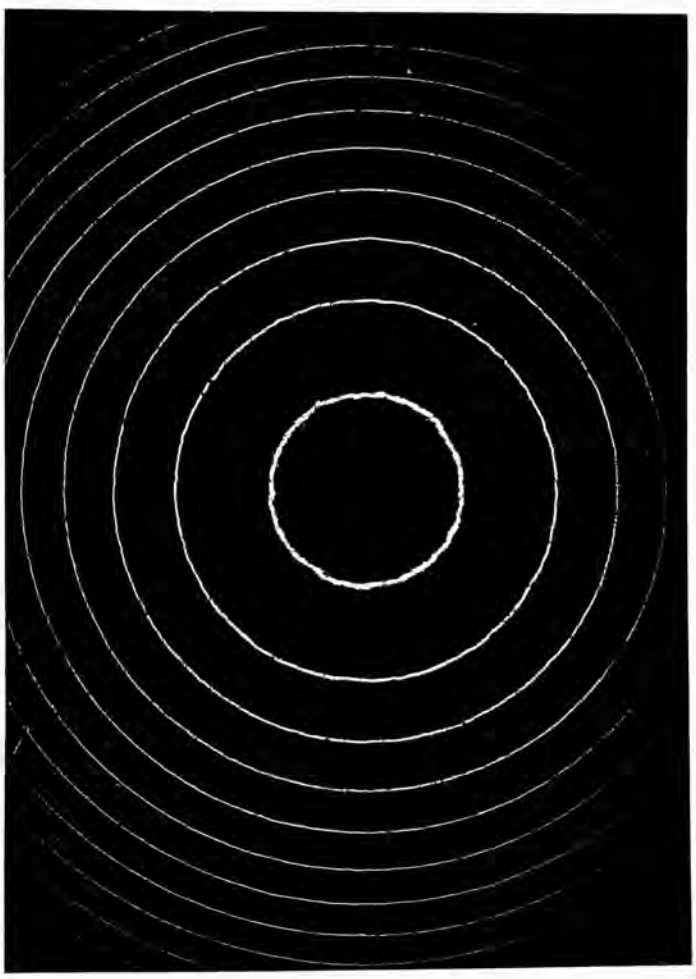

Fig. 8. Multiple Beam Newton's Rings in Transmission.

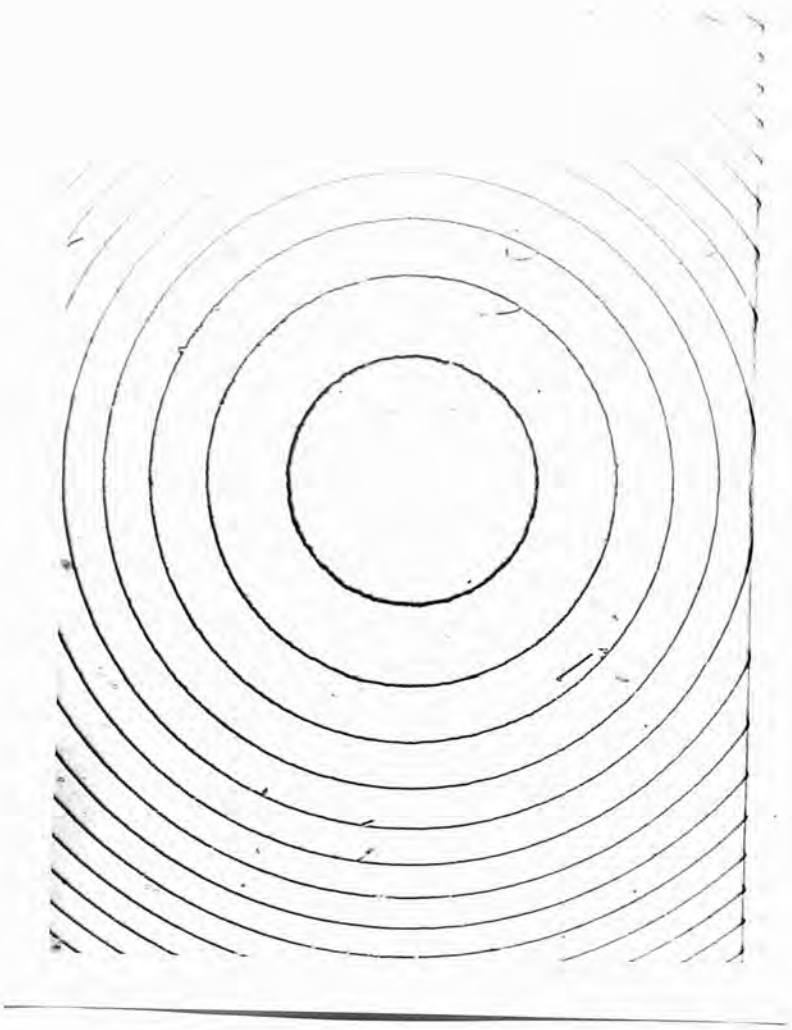

Fig. 8a. Newton's Rings in Reflection.

Fig. 9. Trigons on Diamond - Fizeau Fringes.

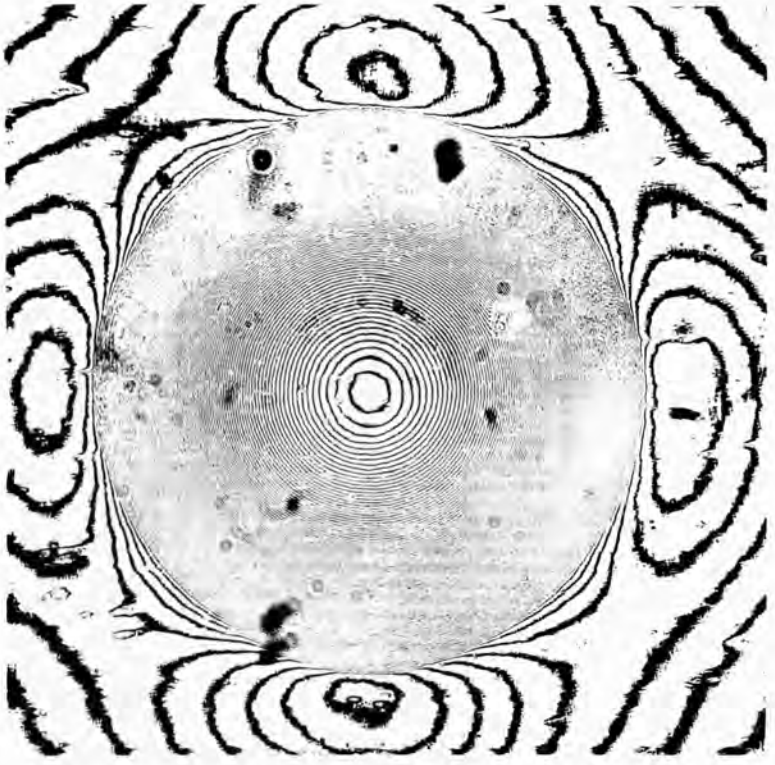

Fig. 10.
Spherical hardness indentation on brass, showing a spherical hollow surrounded by four hills.

We will now examine in detail the properties and methods of formation of these multiple-beam Fizeau fringes. The optical conditions necessary for their observation are discussed at length. This is done for the case of the transmission system, as the theory of this is rather more straightforward. A later chapter deals with the reflection system in particular, and it is pointed out how and where reflection theory can draw from the study of transmission fringes and where it differs.

Transmission Multiple Beam Fringes.

We will now consider how multiple beam interference fringes are formed in a wedge of air between two silvered glass flats. Since the wedge is of air we can neglect the changes of direction produced by refraction in the glass from our calculations. Let a parallel beam of monochromatic light fall upon the film at normal incidence. The film is bounded by NO and LM. Rays CD and IJ will pass on through the film with loss of intensity consequent upon transmission through the two silvered layers NO and LM. Consider also the rays ABED and FGMJ, which meet the rays CD and IJ in the front

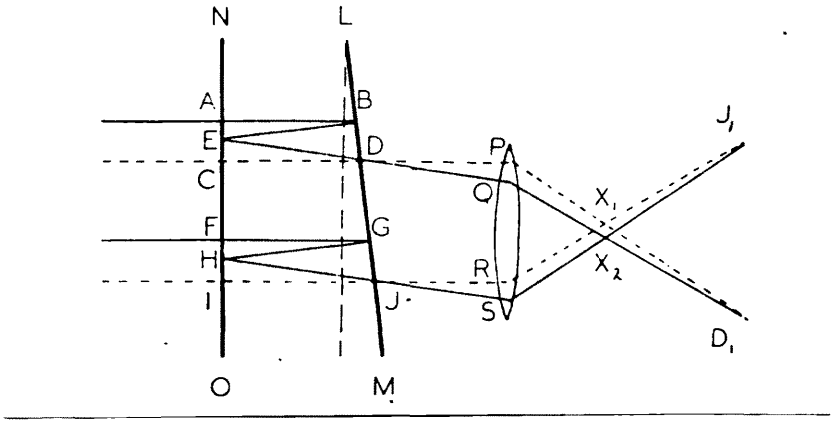

Fig. 11

surface. Since the pairs of rays meeting at D and J are coherent, we will have steady interference effects at D and J. These points are imaged by the microscope objective in the plane conjugate to LM at J_1 and D_1. For a perfect lens, the phase relationships holding at D and J will be exactly

reproduced at J_1 and D_1. So we will see interference fringes in the plane of J_1 and D_1. It is seen that the fringes formed in this way are localized in the thin air film. This important fact means that we can examine the topography of either of the two surfaces bounding the film, provided of course that one of the two is an optical flat.

We will now show that, for low orders of interference, the intensity distribution in the air wedge of these Fizeau fringes of equal thickness is the same as in the well known Fabry-Perot type fringes of equal inclination, but with t as the variable parameter instead of θ.

This was first demonstrated by TOLANSKY 1946 (c), and later discussed by TOLANSKY 1948 (a), and by BROSSEL (1947. Brossel, in 1947, gave what is now the standard treatment of the problem. It is useful in that it lays emphasis upon wavefronts rather than upon rays. It thereby lends itself to more general applications, such as interference in the higher order Feussuer sufaces.

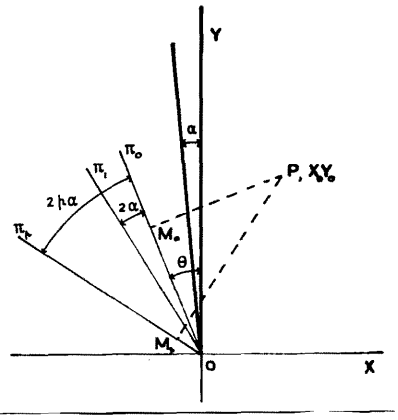

Fig. 12

Fig. 12 represents a wedge, of which one reflecting surface is OY, and the other is at a small angle α to this. OX is drawn perpendicular to OY. The third axis OZ will be in the junction of the two wedge faces. Thus the plane YOX is considered to be a principal section of the wedge. If now a wavefront meets the wedge, with its normal in the plane YOX, and making an angle θ with OX, a family of wavefronts $\pi_0, \pi_1, \pi_2,$ will be formed due to muntiple reflections at the wedge faces. They will make angles θ, $\theta + 2\alpha$, $\theta + 4\alpha$, ... $\theta + 2p\alpha$, ... with OY, as shown.

Apart from phase changes on reflection (which we will assume, for simplicity, will be the same at both wedge faces), all the wavefronts will be in phase at the apex O. If the phase change on two reflections is $\frac{2\pi}{\lambda}\beta$, the difference in phase between the direct and p^{th} wavefront when they pass a point P $(X_0\ Y_0)$ is,

$$\delta_p = \frac{2\pi}{\lambda}(M_pP - M_0P + p\beta)$$

$$\text{i.e. } \delta_p = \frac{2\pi}{\lambda}\left[X_0\cos(\theta + 2p\alpha) + Y_0\sin(\theta + 2p\alpha) - X_0\cos\theta - Y_0\sin\theta + p\beta\right]$$

$$\therefore \delta_p = \frac{2\pi}{\lambda}\left\{(Y_0\cos\theta + X_0\sin\theta)\sin 2p\alpha - (Y_0\sin\theta + X_0\cos\theta)(1 - \cos 2p\alpha) + p\beta\right\}$$

Now we put

$$\sin 2\mu d = 2\mu d + \tfrac{4}{3}\mu^3 d^3$$

$$\downarrow \quad \cos 2\mu d = 1 - 2\mu^2 d^2$$

$$\therefore \quad \delta_\mu = \frac{2\pi}{\lambda}\left[(\gamma_0\cos\theta - \chi_0\sin\theta)(2\mu d - \tfrac{4}{3}\mu^3 d^3) - (\gamma_0\sin\theta + \chi_0\cos\theta)(2\mu^2 d^2)\right]$$

If we neglect the fourth and higher powers of pd, becomes,

$$\delta_\mu = \frac{2\pi}{\lambda}\left\{\gamma_0\, 2\mu d\cos\theta\left[1 - \tfrac{2}{3}\mu^2 d^2 - \mu d\tan\theta\right] - \chi_0\, 2\mu d\sin\theta\left[\mu d + \tan\theta\left(1 - \tfrac{2}{3}\mu^2 d^2\right)\right] + 2\mu\beta\right\}$$

This expression was first derived, for the case $\theta = 0$ by TOLANSKY 1946 (c), and BROSSEL, 1947.

In the case of light at normal incidence, $\theta = 0$ and,

$$\delta_\mu = \frac{2\pi}{\lambda}\left[2\mu t\left(1 - \tfrac{2}{3}\mu^2 d^2\right) + 2\mu\beta\right]$$

when $X_0 = 0$, i.e. on the wedge.

$$\therefore \quad \delta_\mu = \frac{2\pi}{\lambda}\left[\mu(\beta + t) - \tfrac{4}{3}\mu^3 d^2 t\right] \qquad \ldots\ldots (b)$$

Provided we can neglect the term involving the third powers,

$$\delta_\mu = \frac{2\pi}{\lambda}\, 2\cdot\mu\,(t + \beta).$$

This leads to the expression for the transmitted intensity,

$$I = I_0 \frac{1}{1 + \frac{4\Omega}{(1-a)^2}\sin^2\left(\frac{\delta}{2}\right)}$$

$$\delta = \frac{2\pi}{\lambda}(t + \beta)$$

The properties of this expression have been discussed above.

So we see that, provided that $\frac{4}{3}\mu^3\alpha^2 k$ can be neglected compared with $2\mu(k+d)$, we have fringes of equal thickness localized in the film which have the sharp maxima associated with the Fabry - Perot interferometer.

The Third Order Asymmetry of the Fringes.

The effect of having the term $\frac{4}{3}\mu^3\alpha^2 t$ not insignificant can easily be seen from the vector treatment of the Fizeau multiple beam system dye to Faust (1949). The fundamental "Fabry - Perot" calculation involves in essence a summation of an infinite number of S.H.M's of diminishing amplitude and steadily varying phase. This can evidently be achieved by the vector representation method as well. Each of the interfering beams is represented in the diagram by a vector whose length and orientation denote the beam's amplitude and phase. The zero phase is marked by a horizontal dotted line directed towards the right. Phase retardations are signified by anti-clockwise rotation. The vector length decreases geometrically at a rate determined by the effective reflection coefficient of the interferomater surfaces. The resultant amplitude and phase are obtained from the line joining the first to the last vector, but naturally only a finite number of beams can be drawn. Faust assumed that, due to the rapid diminution in vector length with increasing number of reflections, an approximately correct qualitative picture of the interferometer behaviour would be obtained by about 20 - 30 vectors. The vector diagram for the transmission system is shown for four values of δ in the diagram following.

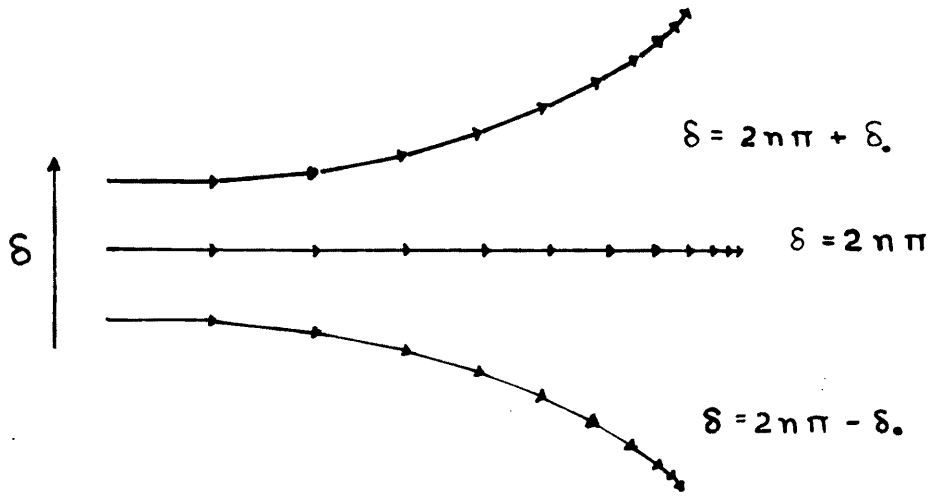
δ = 2nπ + δ₀
δ = 2nπ
δ = 2nπ - δ₀
δ

The full lines in Fig.14 are for the case when the correction term in (6) may be neglected. As a phase retardation is shown as an anti-clockwise rotation, the dotted lines show what happens when the correction term comes into play. The deviation from the ideal case increases as h^3.

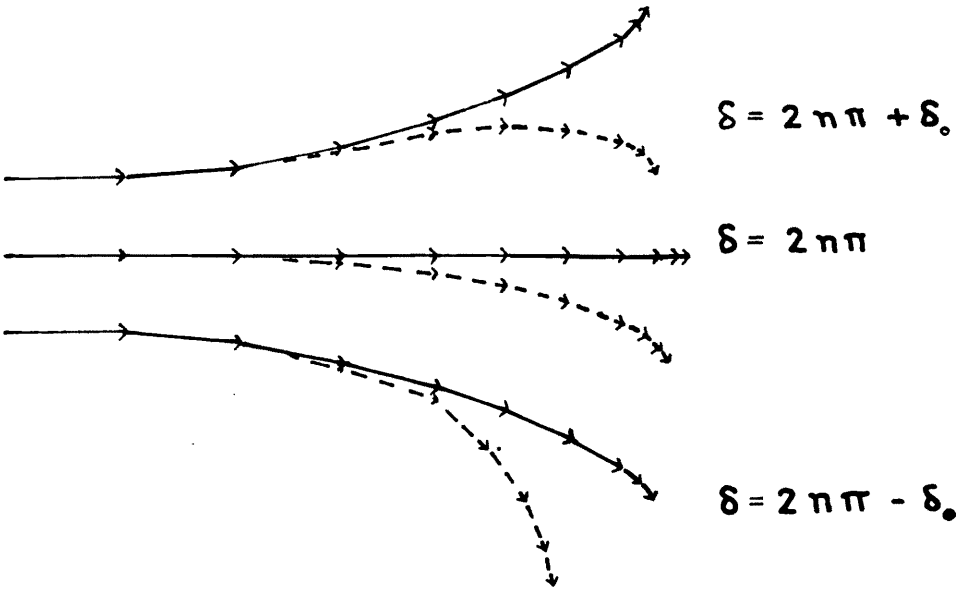

Fig. 14.

Now it can easily be seen by inspection of the vector diagrams that the correction term will have three serious effects upon the interference pattern, namely (see WILCOCK (1951)).

a) The maxima are displaced from their positions as given by (7) away from the apex by an amount which increases with k, so that the distance between adjacent fringes corresponds to a change in wedge thickness of more than $\frac{\lambda}{2}$.

b) The intensity of the maxima is reduced from the value for zero correction, i.e. $T^2/(1-R)^2$ and grows less as to increases.

c) The intensity distribution about the maxima ceases to be symmetrical. This can easily be seen from the series of vector diagrams shown in Fig. 14. The resulting fringe shape is shown below in Fig. 15.

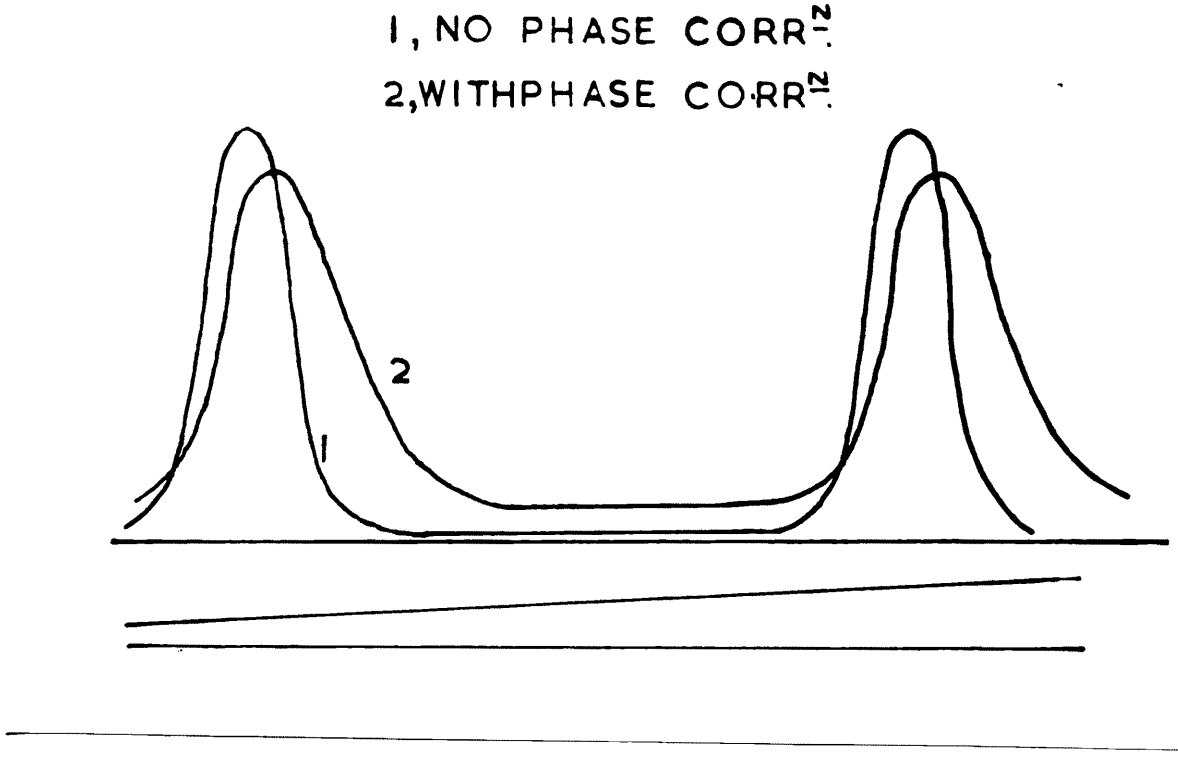

Fig. I5.

Now it is observed that for higher order wedge thicknesses secondary maxima appear in the side of increasing order. These are especially noticeable when the main fringes are sharp. Their formation can be predicted from the vector diagram, thus: at a thickness t, the angle between the vectors of higher h is

$$\phi = 4/3\, h^3 \alpha^2 t$$

and

$$\frac{2\pi}{\lambda}(2t) = 2N\pi + \delta_0$$

So,

$$\phi = \frac{4}{3} h^3 \alpha^2 \frac{\lambda}{4\pi}(2\pi N + \delta_0)$$

Thus ϕ increases as we go from one fringe to the next. It is due to this increase of ϕ as δ_0 increases that the secondary maxima are formed.

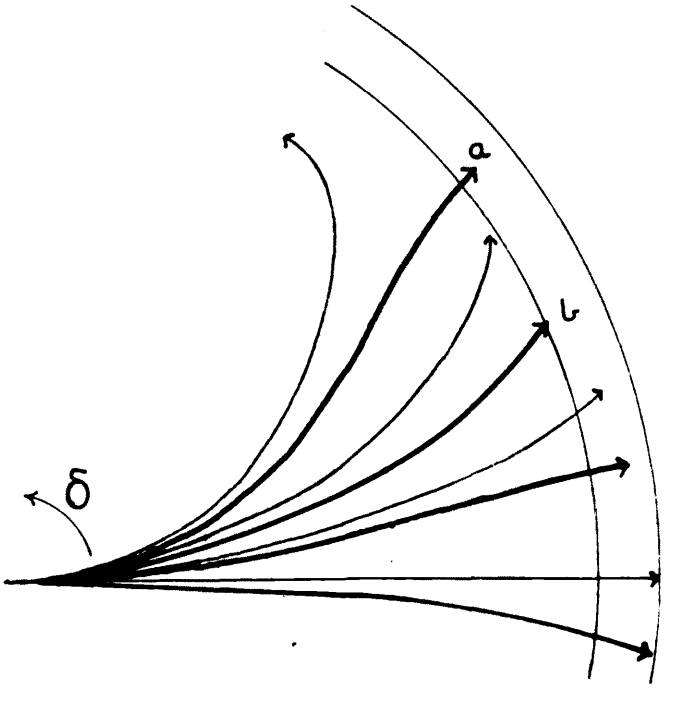

Fig. 16.

Fig. 16 has been drawn to illustrate exactly how this occurs. The thin lines give the positions of the vectors without the phase correction and the full lines apply to the real wedge interferometer. The resultant intensities are given by the lines joining the ends of the vectors to the origin. As we go from one fringe to the next ϕ increases to such an extent that a is further from the origin than b. The intensity will then fall to a near zero value with increase of δ. Hence a secondary maximum is formed.

Experimental Conditions for the Production of High Quality Multiple Beam Fizeau Fringes.

To obtain high quality multiple beam Fizeau interference fringes certain experimental conditions must be adhered to. These have been discussed widely in the literature - see TOLANSKY, 1948, 1946(c), and 1955, and WILCOCK, 1951. They are really quite simple conditions, and high quality fringes can be obtained with apparatus which is by no means complex. The high resolution in depth - of the order of molecular dimensions - that can be secured with quite simple apparatus is remarkable when one considers the elaborate nature of the apparatus, the electron microscope, which is required to secure such high lateral resolutions. We will now enumerate and discuss the conditions under which multiple beam Fizeau fringes can be observed.

A. The Surfaces Must Be Coated With A Highly Reflecting Film.

As mentioned above we will only consider the transmission fringe pattern here, leaving the reflection case for special consideration later.

For low order interference, the correction term $\frac{4}{3}\mu^3\alpha^2 k$ is small in any system which would be used in practice. So the fringe intensity distribution is

$$I = \frac{I_o}{1 + \frac{4R}{(1-R)^2}\sin^2\frac{\delta}{2}}$$

in which $I_o = T^2/(1-R)^2$ is the maximum of

the pattern. To discuss the effect of the constants of the silver film, i.e. of the reflection, transmission and absorption coefficients upon the sharpness of the fringes, we define a half-width w, to be the order separation between points whose intensity is half that of the maxima. To find w, we put

$$\frac{I_0}{2} = \frac{I_0}{1 + \frac{4R}{(1-R)^2} \sin^2 \frac{\delta_\omega}{2}}$$

$$\therefore \quad \frac{(1-R)^2}{4R} = \sin^2 \frac{\delta_\omega}{2}$$

For sharp fringes, we can put $\frac{\delta_\omega}{2} = \sin \frac{\delta_\omega}{2}$,

$$\delta_\omega = \frac{1-R}{\sqrt{R}}$$

and $$\omega = \frac{2\delta_\omega}{2\pi}$$

$$\therefore \quad \omega = \frac{1-R}{\pi\sqrt{R}}$$

Thus the half-width as a fraction of our order is $1-R/\pi\sqrt{R}$, and so increases as R increases.

The maximum intensity on the other hand is $T^2/(1-R)^2$, for unit incident intensity. This is unity when $T+R=1$, i.e. $A = 0$, but less than unity when $A \neq 0$. It is evident that the shape of the fringes depends only upon R , but that the intensity scale with respect to the incident illumination is determined by the fraction $T^2/(1-R)^2$

We see then that the position is:-

a) High values of R give sharp fringes,

b) but higher values of R entail, in general, higher values of A (this statement will be qualified later), and so a reduction in overall intensity.

A compromise has to be reached between these two in practice, but we are helped considerably by the low chromatic resolving power of very low order fringes. Thus a high pressure source can be used and a reduction of up to 50% in intensity can be tolerated.

A later section will deal with the way in which the R, T, and A of metallic and mutilayer films behave.

B. The surfaces must be very close together, i.e. we require a very thin wedge.

This is the essential point upon which the use of sharp muntiple beam fringes for the study of surface topography rests. It was realized from the outset and is mentioned in the earliest literature, e.g. TOLANSKY, 1944 and 1946(c), and is emphasized in the later books TOLANSKY, 1948 and 1951. There are four reasons why this is such an important desiratum for the production of the sharpest fringes.

The first concerns the phase-lag term calculated above. We recall that this is

$$\frac{4}{3} n^3 \alpha^2 t$$

showing that it is proportional to the film thickness t . We now consider a critical thickness t_c , such that, for the number of beams collected by the microscope, the phase lag for the last beam is $\lambda/2$. (The number of beams collected depends on the reflectivity, the wedge angle, and the numerical aperture of the objective - but at low powers mainly on the reflectivity. Up to 60 effective beams may be collected in certain cases. This will be discussed later in this section.)

So:- $$\frac{4}{3} n^3 \alpha^2 t_c = \frac{\lambda}{2}$$

Now we have to have at least two fringes in the field of view, otherwise we cannot make any calculations of fringe dimensions and displacements in terms of order fractions. Thus X , the number of fringes per centimeter, has a minimum value for the magnification used to view the fringes. We have also the relation

$$\alpha = \frac{\lambda}{2} X$$

So:- $$t_c = \frac{3}{2 n^3 \lambda X^2}$$

The accompanying table gives values of t_c and X assuming $n = 60$. Now t has to be less than this to prevent a loss in fringe definition due to the phase-lag term. We note that as the magnification increases, so does the severity of the

restriction on the film thickness.

No. of fringes per cm. X	1	10	100
Critical t, mm.	1.26	.012	.0001

The second important point is the effect of film thickness on the linear displacement of the beams combining to form the pattern. There are two dangerous effects here. By reference to the figure below it can be seen that if the displacement of

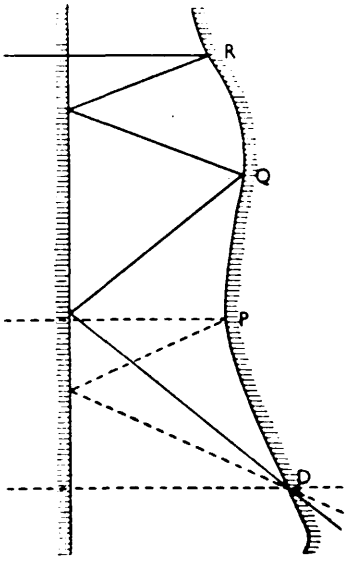

Fig. 17

the higher order beams is too large, their phases will be quite arbitrary with respect to the direct beam. This will reduce the fringe definition considerably in many practical cases. Also UNLESS THE MAJORITY OF THE BEAMS COME FROM

AN AREA LESS THAN THE AIRY DISC (in the object space) OF THE GIVEN OBJECTIVE WHICH IS BEING USED TO VIEW THE SURFACE, THEN THE FRINGE PATTERN DOES NOT NECESSARILY GIVE A TRUE REPRESENTATION OF THE SURFACE TOPOGRAPHY. If the area over which the beams are being collected is larger than the Airy disc in the object space, then it is quite likely that fake information will be given, i.e. the information will not be that at a point on the surface, but the averaged information over a finite area. Moreover, provided that this condition is obeyed, then we can say that we are getting information about a point on the surface, subject of course to the limitation that we have no empty magnification.

An approximate calculation of this effect for small angles follows.

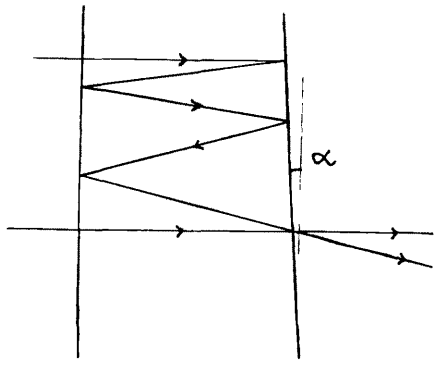

Fig. 18

Consider a beam which has suffered n reflections at the "back" surface before it reaches the point of observation.

Then the total line or displacement of this beam is

$$d_n = 2t\left[2n\alpha + (2n-1)\alpha + \cdots + (2n - \overline{2n-1})\alpha\right]$$

$$= 2t\alpha\left[n^2 - (1+2+3+\cdots+\overline{n-1})\right]$$

$$= 4t\alpha\left[n^2 - \frac{n-1}{2}(1+n-1)\right]$$

$$\therefore \quad d_n = 2t\alpha n(n+1)$$

So for $n \gg 1$,

$$d_n = 2t\alpha n^2 \qquad (9)$$

Thus, since d_n is proportional to the film thickness, it has to be kept as small as possible by reducing t.

At medium powers we find, from the following simple calculation, that, provided the film thickness is less than the critical value t_c calculated above, all the beams come from an area which is less than the Airy disc in the object space. For we have,

$$d_n = 2n^2 t\alpha$$

And,

$$\alpha = \lambda x \;, \quad t_c = \frac{3}{2n^3 \lambda x^2}$$

So,

$$d_n = \frac{3}{2nx}$$

The table above gives values of t_c and X for $\gamma = 60$. Using $\gamma = 60$ and X = 100 fringes per cm.,

$$d_{60} = 2.5 \times 10^{-5} \text{ cm.}$$

This is within the Airy disc of a medium powered microscope.

The use of such thin films, of the order of a few wavelengths thick, has the further important advantage that the chromatic resolving power of the system is very low. The fundamental formula governing the position of the maxima is

$$m\lambda = 2\mu t \qquad \text{(for normal incidence)}$$

So $$\nu = \frac{m}{2\mu t}$$

where $\nu = 1/\lambda$ is the wavenö corresponding to λ

Thus the wavenumber separation between orders is $\Delta\nu = 1/2\mu t$

For $t = .001$ mm. , and $\mu = 1$, this is,

$$\Delta\nu = 5000 \text{ cm.}^{-1}$$

So for a wavelength of 5000A . ($\nu = 20{,}000$ cm.$^{-1}$), the neighbouring maxima occur at 15,000 and 25,000 cm.$^{-1}$ respectively, i.e. at 6666 A. and 4000 A. . In this case the wavelength separation between orders is about 2000 A . It is found in practice that even the best fringes are no more than 1/50 th of an order wide. This corresponds in this case

to about 30 Å . This is somewhat greater than the line widths at about 5000 Å , of ordinary mercury arcs. So we see that the question of source line widths is of little consequence here thanks to having a very thin air film. This means we are at liberty to use high pressure arc sources to overcome intensity troubles met with highly reflecting films, both silver and mutilayer.

A further point of interest is the divergence of the multiply - reflected beams from the axis of the microscope with respect to the aperture of the objective. We shall see that in all normal cases, enough beams are collected to make a fair Fabry-Parot type intensity distribution. Suppose that the semi-angle of the cone of illumination entering the microscope is u , i.e. the numerical aperture (N.A.) is $\mu \sin u$. The divergence of the p^{th} beam from the microscope axis is

$$\psi_p = 2p\alpha$$

where α is the wedge angle between the surface under test and the flat.

We will now calculate the minimum angle α foragiven objective, to give at least three fringes in the field of view. Then

$$\alpha_{min} = \frac{\lambda}{s}$$

where s is the diameter of the field of view in the object space. Suppose further that the field of view in the image

space has a diameter of 10 cm. Then taking a magnification of 750 times the numerical aperture of the objective,

$$d_{min} = 75 \times (N.A.) \times \lambda \qquad (10)$$

So, $\psi_h = 150\, h \cdot (N.A.) \cdot \lambda$

Let h_o be the greatest number of beams that can be collected by the objective. Then:-

$$\sin^{-1}(N.A.) = 150\, h_o\, (N.A.)\, \lambda.$$

$$\therefore \quad h_o = \frac{\sin^{-1}(N.A.)}{150 \cdot (N.A.) \cdot \lambda.} \qquad (10a)$$

The following table gives corresponding values of h_o and N.A. for $\lambda = 5 \times 10^{-5}$ cm. Approximate values only are given.

N.A.	h_o
.2	130
.25	130
.5	136
.75	145

Now the intensity distribution in a Fabry-Perot set up

when only a finite number, n, beams is collected is,

$$I = \frac{(1-R^n)^2 + 4R^n \sin^2(\pi\delta n/\lambda)}{(1-R)^2 + 4R\sin^2(\pi\delta/\lambda)}$$

This reduces to the familiar Fabry-Perot distribution when $R^n \ll 1$. Fig. 19 below shows how R^n varies with N for two high, but typical values of R. Actually R^{2n} is plotted here, but it can be seen that when n is of the order of 100, we will have a narrow "infinite beam" distribution to all intents and purposes.

It was pointed out above that, for a given air gap, t, fringe definition falls off with increasing magnification. This variation is now investigated using the calculation of α_{min} given above. The third order term δ for a gap t is

$$\delta_n = \frac{4}{3} n^3 \alpha^2 t$$

When $\alpha = \alpha_{min}$

$$\delta_n = \frac{4}{3} n^3 t \cdot .75^2 \lambda^2 (N.A.)^2$$

Putting $t = \lambda/2$

$$\delta_n = .2450\, n^3 \lambda^3 (N.A.)^2$$

The graph (Fig.20) shows δ_n as a function of N.A. for $n = 60$, i.e. the phase lag for the sixtieth beam is plotted against N.A. For objectives of numerical aperture up to .5 it is

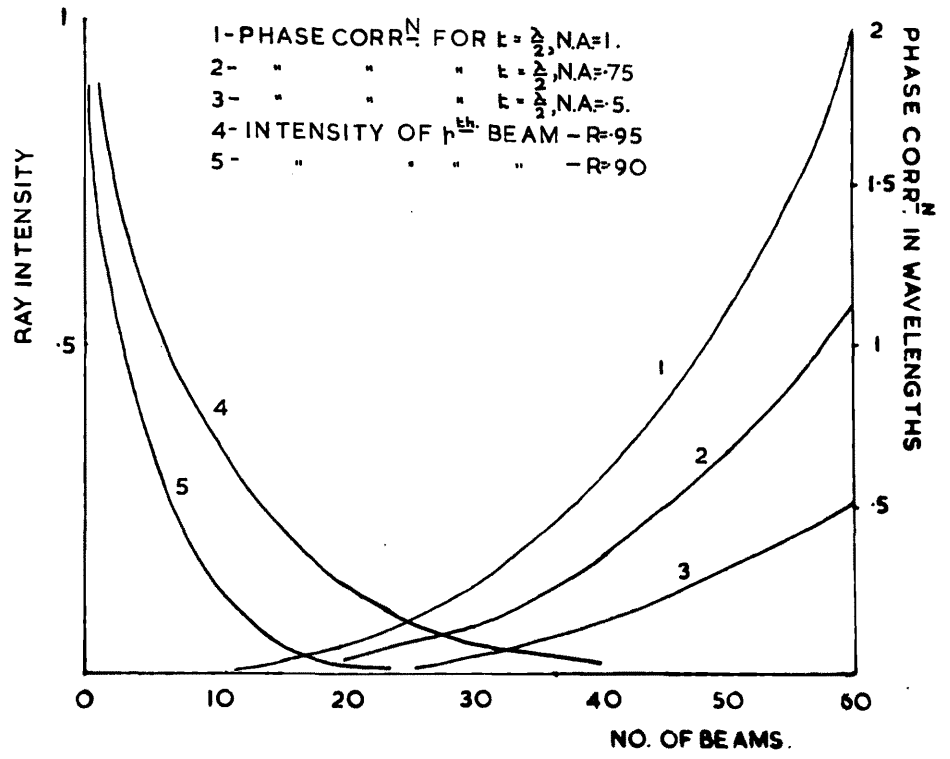
1-PHASE CORR^N FOR t = λ/2, N.A=1.
2- " " " t = λ/2, N.A=·75
3- " " " t = λ/2, N.A=·5.
4- INTENSITY OF n^th BEAM – R=·95
5- " " " " – R=90
RAY INTENSITY
PHASE CORR^N IN WAVELENGTHS
1
·5
2
1·5
1
·5
0
10
20
30
40
50
60
NO. OF BEAMS.
1
2
3
4
5

Fig. 19.

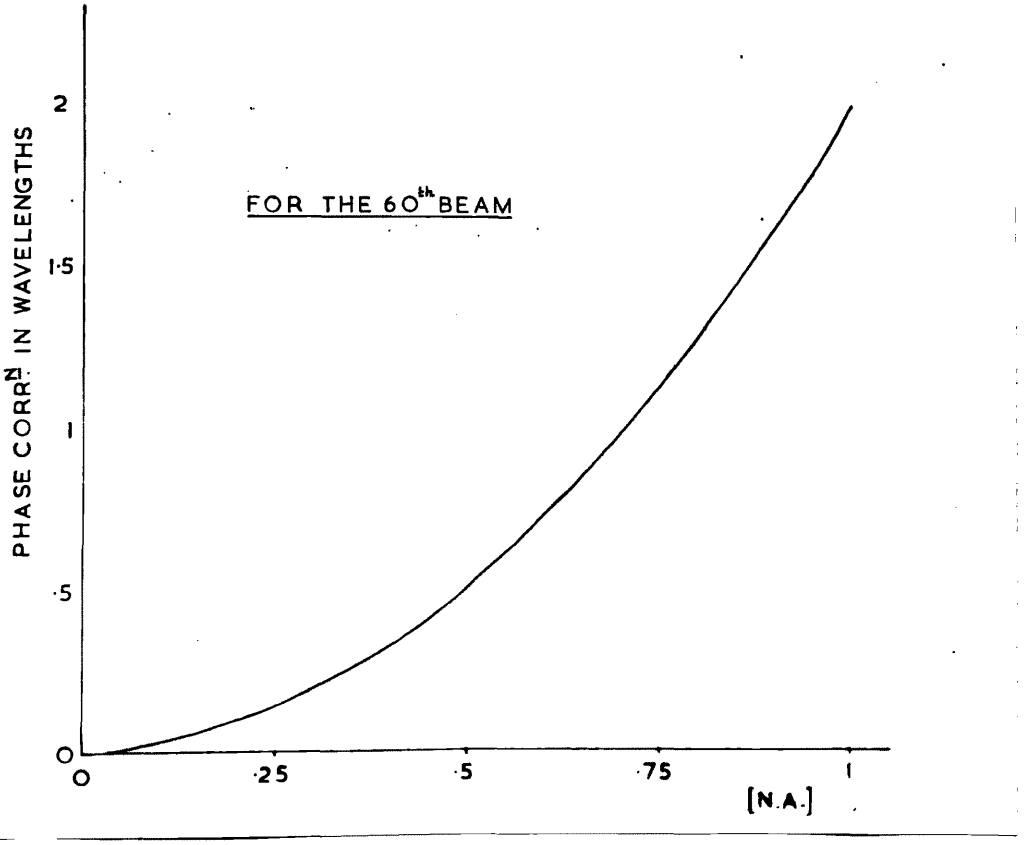
FOR THE 60th BEAM
PHASE CORR^N IN WAVELENGTHS
2
1·5
1
·5
0
·25
·5
·75
1
[N.A.]

Fig. 20.

seen that fringe definition is excellent, for even the sixtieth beam, which has a very low intensity indeed, has a phase lag of only $\lambda/2$. However it seems at first sight that at higher magnifications fringe definition suffers considerably. The first graph, Fig. 19, shows that this is not necessarily so in fact. Here the phase lag is plotted against the number of beams, n for different N.A.'s. On the same graph is plotted the intensity of the n^{th} beam, R^{2n}, for two typical values of R, .90 and .95. Consider the case of N.A. = 1, the most severe one. Nearly two-thirds of the beams have a phase lag of less than $\lambda/2$ and those that have a greater phase lag have such low intensities that they do not exert a great effect upon fringe definition. Thus we may expect to obtain fringes with reduced but by no means poor definition. This has been shown to be the case by TOLANSKY and EMARA, 1955, who show the first two orders of a " Newton's Rings" arrangement obtained on a diamond face. Of course when t increases fringe quality will suffer, and again we see how small t must be, especially at high magnifications. On this same graph are plotted the (phase lag) - (number of beams) curves for N.A. equal to .75 and to .5. When N.A.= .5 no difficulty is met at all, and this is the strongest recommended objective for use with multiple beam surface interferometry, unless exceedingly thin air gaps can be obtained, which is by no means always the case.

For high powered objectives at the thin air gaps considered here, and for lower powered objectives if we are forced to have rather larger air gaps, it is likely that the phase lag- ϕ curve will rise above half a wavelength for higher values of ϕ. The behaviour of such a system can be visualized by an idea due to Dr. V.G. Bhide of this Laboratory. He supposes that we have an approximate Airy distribution due to those beams which have phase lag less than $\frac{\lambda}{2}$ and another, $\frac{\lambda}{2}$ out of phase with the first, for the succeeding beams which have phase lag in the range $\lambda/2 < \delta_h < \lambda$. The maximum of this latter distribution will of course be much less than that of the former, giving an approximately true Airy distribution.

It is also of interest to calculate the maximum useful N.A. with this system by equating the diameter of the objective diffraction disc with the displacement of the last effective beam along the surface. The displacement d_h is

$$d_h = 2h^2 k\lambda$$

So,

$$\frac{\lambda}{N.A.} = 2h^2 k .45 . \lambda \, (N.A.) \quad , \text{ for } d = d_{min}$$

$$\therefore \quad (N.A.)\ max. = \frac{1}{\sqrt{150 k}\ h}$$

If now we suppose that beams above the twentieth will not contribute greatly to the way in which a fringe contours a surface, (see Fig. 19, curve 5), then the maximum value of N.A. permissible will be .82. (Taking μ as 30 this is .55)

To sum up, it has been shown that in order to obtain good fringe definition the air gap must be kept as low as possible due to (a) the third order phase correction term, (b) the beam displacement along the surface, and (c) the finite width of the source line. This is one of the most important features of the multiple beam interferometry of surfaces. The calculations using the value $d_{min} = 45.\lambda.$ (N.A.) show, in the first place, that all the beams of any effective intensity enter the objective for all normal numerical apertures employed. Further, the fringe definition falls off as the microscope magnification increases as $(N.A.)^2$. It is advisable to use only magnifications below X350 where possible, but, provided that the air gap is extremely thin, fringes with rather reduced quality can be obtained up to magnifications of X1000. Also at low powers (below X350), no trouble is met with over large beam displacements. They are well within the Airy disc for all beams but those of negligible intensity. Use of higher magnifications, however, requires care.

C. The Incident Beam Must be Accurately Collimated.

In 1922 Fabry (1922), drew attention to the possible

broadening of interferometer fringes due to incorrect collimation of the incident beam. Errors in collimation can arise from either, (a) lens aberrations or (b) finite source size. Case (a) is complex, and a general treatment has not as yet been given. Case (b) has been discussed by TOLANSKY, 1946(c), 1948, BROSSEL 1947, and HOLDEN, 1951.

We follow BROSSEL's treatment here, but that due to TOLANSKY, although less general, deals with the more important factor. The general calculation of the phase of the reflected wavefront with respect to that of the direct beam gives

$$\delta_p = 2\mu t \cos\theta \left(1 - \mu\alpha\tan\theta - \frac{2\mu^2+1}{3}\alpha^2\right) \qquad (11)$$

When θ is of the same order as α, then the $\tan\theta$ term in (11) may be neglected, and we have a fringe broadening due to the $\cos\theta$ term alone. This will give a square topped distribution, the maxima corresponding to the higher values of θ being displaced away from the wedge apex. If the fractional order broadening which can be tolerated is Δm, then at the order of interference n, the angular radius of the source must be less than

$$\beta = \sqrt{\frac{2}{n}\Delta m} \qquad \text{see TOLANSKY, 1946(c)}$$

For small gaps, we have to use large values of θ to produce a given Δm. At large angles of incidence, the $\tan\theta$ term comes into play, and this gives a wing on the side of

increasing . This fact has been verified by microphotometering fringe intensity distributions, (BROSSEL, 1947). The results are shown in Fig. 21. Curve I shows the natural width - highly collimated beam, curve II is for small θ values, and curve III shows the effect of the $\tan\theta$ term.

Since the wing occurs only on the side of increasing t, it occurred to Brossel to use a convergent beam as a means of solving the "hills or valleys" question. (BROSSEL, 1946)

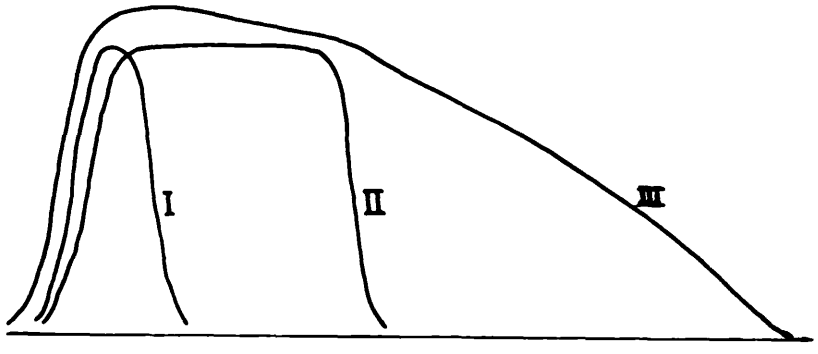

Fig. 21.

To use this method for sorting out a topography, a highly convergent beam must be used. If only smallish angles are employed the $\tan\theta$ term will not operate. The figure following shows a set of fringes with (a) well collimated

light and (b) convergent light.

Fig. 22.

TOLANSKY (1948) has given a table of tolerances for collimation, giving the film thickness t, and the corresponding angular deviation, θ, from the normal for a phase shift of 1/5 the half width. It is reproduced below.

t (mm)	1	0.1	0.01	.001
θ^{o}	$^{1}/_{10}$	$^{1}/_{3}$	1	3

The calculation is based on the small angle broadening only which is the practical case. This table illustrates the fundamental rule that, for good fringe definitions small values of t should be used, for the collimation conditions are far less stringent when small values of t are employed.

WILOCK, 1951, discusses the tolerance in phase shift due to collimation errors with regard to the natural half-widths of a line (ω). He again points out that, in practice the $\tan\theta$ term may be neglected. He basis his calculations upon the work of Dufour and Picca (1945) on the broadening of Fabry-Perot fringes. Let the order shift be Δn. Then if $\Delta n \ll$ the natural width, increase of θ merely increases intensity, while for $\Delta n \gg$ natural width, increase of θ entails only a square topped fringe broadening and no intensity increase. He plots a graph of resultant width / natural width against

Δm / natural width, ($\Delta m = n\beta^2/2$). It is possible to decide from this graph when a suitable transistion point from the condition of increasing intensity (graph horizontal), to that of increasing width (graph sloping at 45°) takes place, and draw up a table similar to that given above for the ratio (Δm / natural width) chosen. It will be seen that TOLANSKY's choice is a reasonable one.

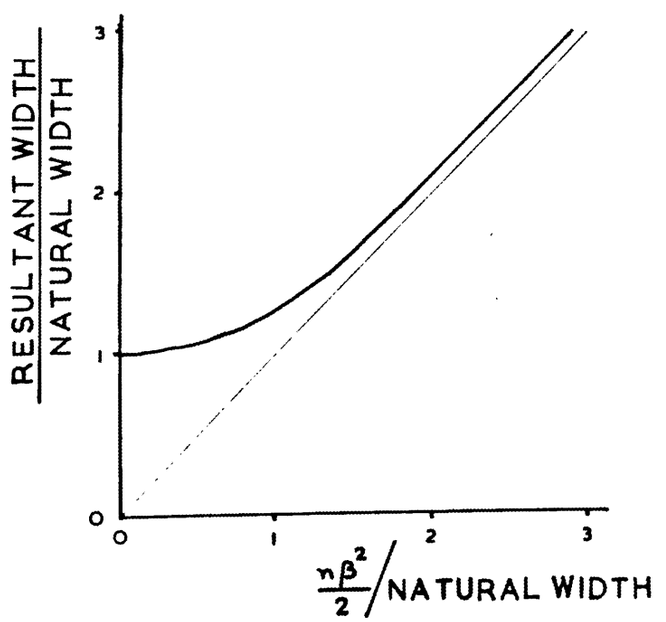

Fig. 23.

The other is:-

D. The incidence should preferably be normal.

Non-normal incidence introduces two complications. At non-normal incidence, the Feussner surface, (FEUSSNER 1927) is not coincident with the plane of the film, its distance from the film, at an angle of incidence, i, is

$$x = t/\phi \frac{\sin i \cos^2 i}{\mu^2 - \sin^2 i}$$

in which t is the film thickness and ϕ the wedge angle.

Now it is evidently of great convenience, when we are studying the topography of a surface to have the fringe system located in the surface itself. This, as we see from the above expression, is only true for $i = 0$.

The other effect of illumination at angles other than zero incidence has been described by TOLANSKY (1944(a)). That is the differential phase change on reflection between light prolonged at right angles and parallel to the plane of incidence. This effect is shown in an elegant manner by viewing the transmission fringes produced in the film between a plano-convex lens and a flat, the surfaces being silvered of course.

This is of course the Newton's Rings apparatus. Here it is used at non-normal incidence, as in the figure below -

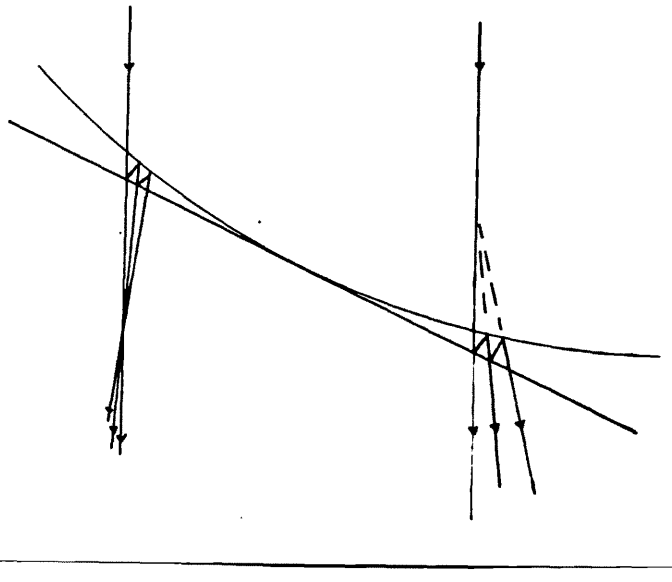

Fig. 24.

To start with, the fringes are elliptical, not circular, as with normal incidence. Also only a small number of them are in focus on a plane perpendicular to the plane of incidence. The most striking observation, however, is that the rings are doubled, as shown in the picture following - (part B only).

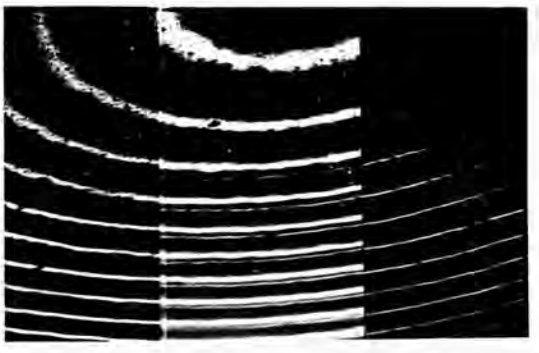

(C) (B) (A)

Fig. 25.

The separation and fringe definition varies with angle of incidence and the outer higher order fringe becomes progressively weaker as it moves away from the other. Now in the figure above, taken with a triple shutter (see TOLANSKY 1948), the two outer portions were taken with a polaroid set to pass vibrations in the plane of incidence (A), and perpendicular to the plane of incidence (C). The middle portion is without a polaroid at all, showing the doubling normally seen (in this picture the weaker component, in A, has been given a longer exposure than the rest of the plate. The correct intensity ratio is shown in B). The angle of incidence here is 60°

Now it is well known from classical electromagnetic theory that the phase change on reflection at a metallic surface is not the same for rays polarized perpendicular and

parallel to the plane of incidence. The plate above shows clearly that this is the cause of the fringe doubling effect at non-normal incidence.

This provides a simple method for measuring the differential phase change. The results obtained by this method were compared with the classical theory of MACLAURIN, 1906.

Appendix to Chapter I

Multiple Beam Interference Contrast.

Tolansky and Wilcock, 1946 and Tolansky, 1948 have described an elegant technique for examining structure in nearly plane surfaces. It employs the interference contrast seen when the surface under test and the flat are brought close and so parallel that the dispersion increases until only one fringe covers the whole of the field of view. The rate of change of intensity varies from zero when the intensity is a maximum, increasing through the point of inflexion at about $I = I_{max}/2$ and going to nil when the Airy intensity drops to zero. Unfortunately this latter region covers quite a large range of thickness but the position is considerably improved by employing an unfiltered arc, or even an unfiltered arc with an impurity, e.g. cadmium, added. Really useful interferograms can be obtained by taking photographs of these high dispersion fringes with the transmission Fizeau system superimposed. The latter can be obtained quite easily by filtering the arc and increasing the wedge angle. We then have a Fizeau picture with the structure to which it corresponds, shown up in enhanced contrast, superimposed on the plate. So one of the disadvantages of Fizeau, namely that there are large regions inbetween the sharp fringes, is overcome. Fig. 26 shows an example of this.

Fig. 26.

TOLANSKY, 1948, gives a simple calculation illustrating the sensitivity of the method. Suppose that the gap is such that I = I max/2, i.e. we are in the region of maximum sensitivity. Then,

$$\delta = 2/F^{1/2}$$

So,

$$k = \frac{\lambda}{2\pi} 2/F^{1/2}$$

Now the eye can detect a 10% change in intensity easily. So we can detect a change in δ to δ', where,

$$.45 \quad I_{max} = \frac{I_{mean}}{1 + F \sin^2 \delta'/2}$$

$$\therefore \quad \delta' = 2.21 / F^{1/2}$$

$$\therefore \quad t' = \lambda/4\pi \cdot 2.21 / F^{1/2}$$

$\therefore$ The change in t detectable is

$$dt = \frac{.21}{4\pi} \cdot \frac{\lambda}{F^{1/2}} \simeq \frac{\lambda}{60 F^{1/2}}$$

For $R = .94$, this is,

$$dt = 3 \text{ Å}.$$

which is remarkably small.

Precise Topography of Optical Surfaces.

In a recent paper SAUNDERS, 1951, described a technique which employed Fizeau fringes using an order separation of less than $\lambda/2$. He used an unfiltered source and rather high dispersion, but not so high as above. The picture was crossed by four or five fringes of different colours and in general, different orders. Before they could be used for

measurements these orders would have to be found. This was accomplished by comparing the relative separations with a diagram, shown in Fig. 27, giving the positions of fringes of different wavelengths on a thickness scale. This method allows the use of smaller wedge angles than d_{min} calculated above, with consequent increase in fringe quality. It also interpolates in the space between fringes, though not so elegantly as above.

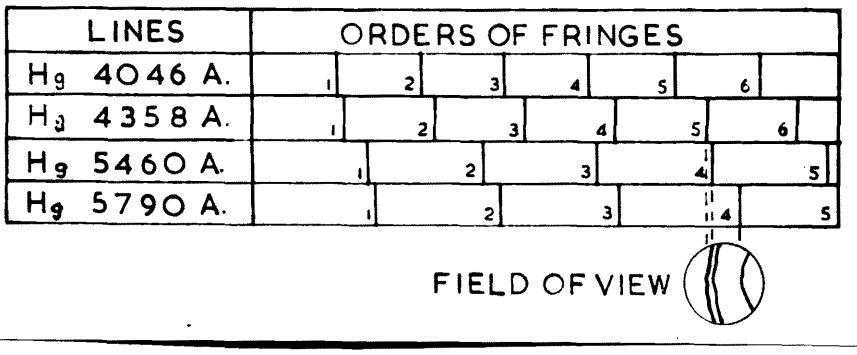

Fig. 27.

The second technique employed by Saunders uses a Fizeau interferometer enclosed in an air-tight chamber. Monochromatic transmission fringes are used and air is slowly pumped from the apparatus - see Fig. 28.

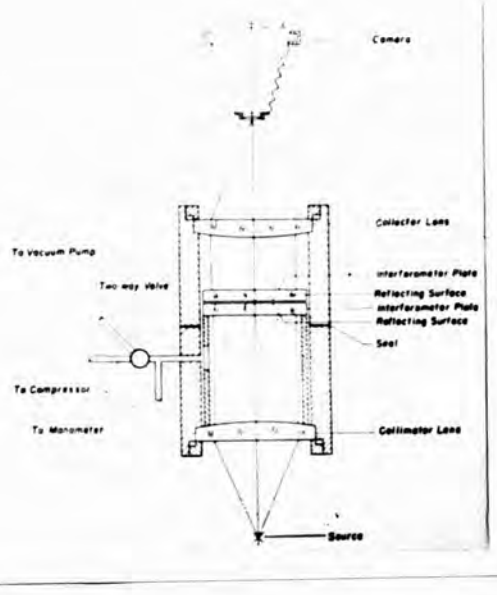

Fig. 28

The fringes slowly move across the field of view as air is removed. Actually air is removed in discrete amounts and the plate exposed when the system is steady. Again the region between the normal fringes is observed and smaller wedge angles can be employed. For quantitative work, it needs a separate calibration interferometer formed between two flats.

CHAPTER II

Reflection Fizeau Fringes.

As stated in the introduction, this dissertation is concerned primarily with the examination of surfaces by reflection methods, as opaque substances are in the majority, and, in any case study of transparent substances by reflection makes the surface examination independant of the bulk structure. (Thin film thicknesses, for example, are evaluated by reflection fringes). However, it was thought best to describe the transmission system, with its simple, symmetrical intensity distribution, first to bring out such features as the effect of small film thickness, the accuracy of the collimation, etc. The rather more complex intensity distribution of the reflected system will be described first, followed by a discussion of the results of Chapter I from the point of view of reflection work.

The Optical Arrangement

Two optical set-ups are employed, the one used depending upon the working distance of the objective. For lower powered lenses, the surface is illuminated by parallel light by a half-silvered beam splitter below the objective. It is desirable to make the splitter as thin as possible, to reduce aberrations in the objective optics introduced by the glass paths, as objectives are not normally designed to work in this

way. This arrangement is shown in Fig. 29.

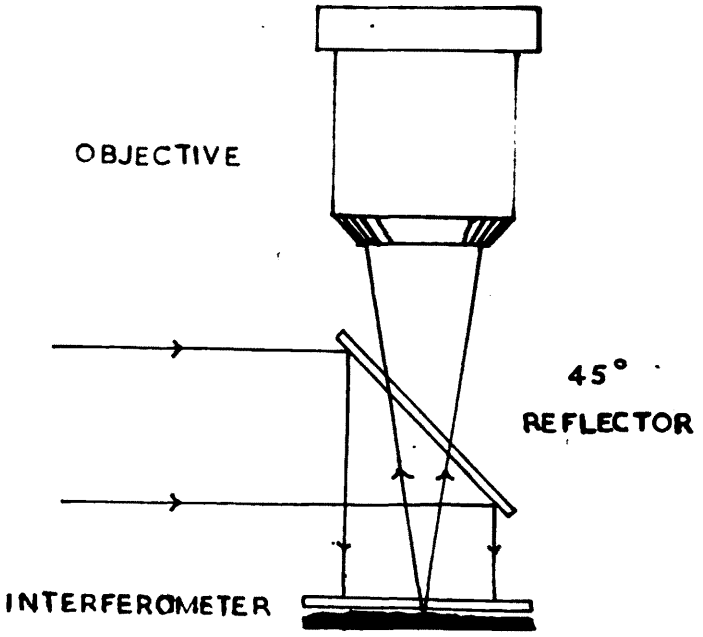

Fig. 29.

For high powered objectives, a conventional metalurgical microscope is employed, as in Fig. 30.

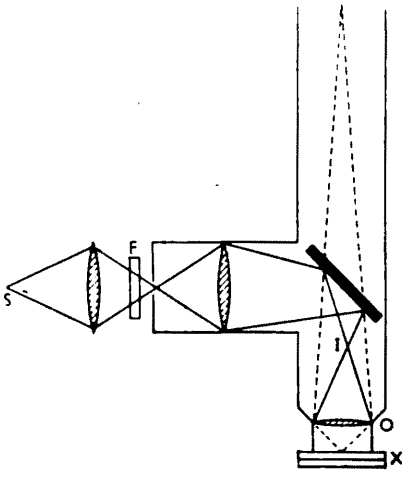

Fig. 30.

The objectives supplied for metalurgical work are generally corrected for use with a glass coated beam splitter, but a further complication is introduced here. It is essential to use a parallel incident beam, and this is secured by arranging to have an image of the point source formed at I, which is the back focus of O. So simultaneously, the objective has to focus on the air film X, (dotted rays) and to produce a parallel beam in the other direction. Thus the demands on the objective optics are severe. (In addition, of course, the objective must be corrected for cover glass thickness) Fig. 31 below is an example of a set of high quality reflection fringes.

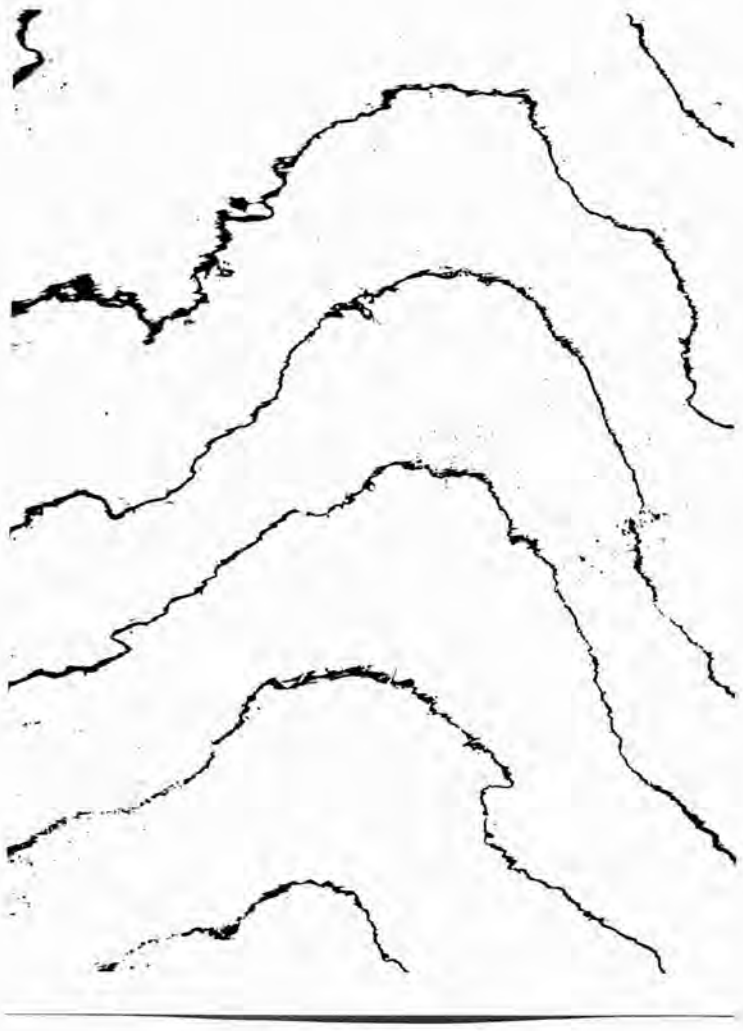

Example of High Quality Reflection Fizeau Fringes

The Intensity Distribution in the Reflected System

This problem was first discussed by HAMY, 1906 and much later by HOLDEN, 1949, in a very thorough article. This section is taken almost entirely from Holden's paper. The first part gives the deriation of the intensity distribution for a parallel plate interferometer in a rigorous manner, assuming that an infinite number of beams are collected but making no reservations upon the symmetry of the interferometer or the range of reflectivities of its two surfaces. The results are extended to the practical case of a thin air gap of wedge shape, by the method described in Chapter I. Only fringes in the zero-order Feussner surface are considered

The results given by Holden were used by him to discuss the variations in fringe appearance one should expect with varying values of the reflectivities of the front and back surfaces. The paper shows clearly how this depends upon the phase conditions at the surfaces as well as upon the reflectivities. These conclusions are verified experimentally and photographs are given in the paper illustrating the effect of varying the reflectivities, the corresponding transmitted and reflected systems being given side by side. A phase quantity, F, which is the sum of the phase changes on reflection (at normal incidence) at the front air-silver interface and the front glass-silver interface, is given for

varying values of the reflectivities. The values of F were calculated from measurements of the fringe displacement from the corresponding transmitted system.

Using these results, Holden found that the value of F for heavily silvered surfaces was $(2n + 1)\pi$, $n = 0, 1, \cdots$ Using this value, the intensity distribution of the multiple beam reflexion Fizeau fringes used in the interferometric study of the microtopography of surfaces is discussed and the effect of absorption in the reflecting films shown. Unfortunately, Holden only discusses a symmetrical ~~interferometer~~ interferometer in this way. In practice, the back surface is heavily silvered while the front one has a 85 to 90% coating, giving a highly asymmetrical set-up. However, the critical effect the absorption in the TOP film has upon fringe quality is shown clearly. The superiority of reflected fringes for precision measurements is clearly demonstrated, so showing that the use of reflected fringes is no drawback in the cases where non-transparent substances are being studied interferometrically. In this section, however, the fringe contrast is defined as $I_{max} - I_{min}$; it might be held that $(I_{max} - I_{min}) / I_{max}$ is a more correct definition.

Holden's calculations of the intensity distribution of the reflected Fizeau fringe system now follows. As stated above, the system first considered is an interferometer bounded by two

plane, parallel, silvered surfaces. Normally incident, monochromatic light gives rise to multiply-reflected beams as shown in Fig. 32.

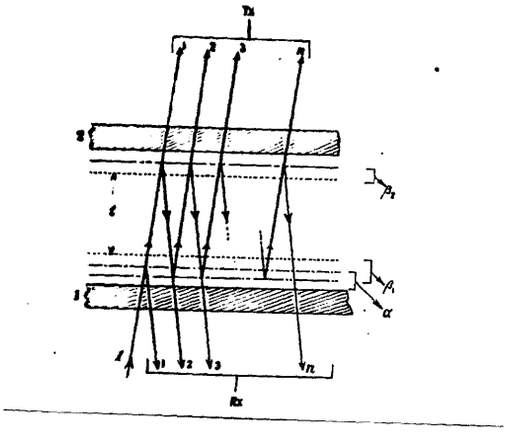

Fig. 32.

The symbols are :-

r_1 & r_2 are the amplitude reflection coefficients at the air-glass interfaces 1 and 2.

t_1 & t_2 are the corresponding transmission coefficients.

β_1 & β_2 are the corresponding phase changes.

r_2 is the amplitude reflection coefficient at the glass-silver interface of surface 1.

α is the corresponding phase change.

The effect of β_1, β_2 and α in reducing the optical separation of the plates is shown in Fig. 32.

Summing the reflected beams gives for the intensity in the focal plane of the collecting lens,

$$I_{RX} = r_2^2 + \left\{ \frac{(t_1^2 r_2)^2 + 2t_1 r_2 r_2 \cos(\delta - \alpha + \beta_2 + 2T_1) - 2t_1^2 r_2^2 r_1 r_2 \cos(2T_1 - \beta_2 - \alpha)}{1 + r_1^2 r_2^2 - 2r_1 r_2 \cos(\delta + \beta_1 + \beta_2)} \right\}$$

In the same nomenclature the transmitted intensity is,

$$I_{TX} = [t_1^2 t_2^2] \times \Theta_\Delta$$

$$= t_1^2 t_2^2 \times \frac{1}{1 + r_1^2 r_2^2 - 2r_1 r_2 \cos(\delta + \beta_1 + \beta_2)}$$

We put the term $(2T_1 - \beta_1 - \alpha) = F$. This is the phase-like term referred to above. It depends only on the first surface. Also we put the optical separation of the surfaces

$$(\delta + \beta_1 + \beta_2) = \Delta$$

So,

$$I_{RX} = r_2^2 + \Theta_\Delta \left[(t_1^2 r_2)^2 + 2t_1^2 r_2 r_2 \cos(\Delta + F) - 2t_1^2 r_2^2 r_1 r_2 \cos F \right] \quad \cdots\cdots (i)$$

This is the intensity distribution, with varying values of the optical separation Δ , of the reflected fringe system.

It is seen that while the transmitted system is described by a magnitude term involving only the transmission factors of the two surfaces, the reflected system has two transmission like terms and one, involving cos $(\Delta + F)$ x Θ_Δ , which gives rise to the differences between the reflected and the transmitted system, (apart from the background term r_2^2).

Holden then proceeds to discuss the positions of the maxima and minima in the reflected fringe system. So:-

For turning points,

$$\sin\Delta\left\{t_1^2 r_2^2 r_1 r_2 + r_2 r_2 \cos F - r_2^2 r_1^2 r_2 r_2 \cos F\right\}$$
$$+ \cos\Delta\left\{r_2 r_2 \sin F + r_1^2 r_2^2 r_2 r_2 \sin F\right\} = 2 r_2^2 r_1 r_2 \sin F \quad -(2)$$

When sin F = o in (1), we see that the roots are equally spaced. So we have maxima halfway in between minima when

a) $F = 2n\pi$

b) $F = (2n+1)\pi$

For the case (a) we have maxima at $\Delta = 2n\pi$ + minima at $\Delta = (2n+1)\pi$

For the case (b) we have minima at $\Delta = 2n\pi$ & maxima at $\Delta = (2n+1)\pi$

Also if we write (2) as

$m \sin\Delta + n\cos\Delta = p$, we see that,

the roots are coincident for

$$F = (2n+1)\pi \; ; \; t_1^2 = \frac{r_2 r_2 \left(1 - r_1^2 r_2^2\right)}{r_2^2 r_1 r_2}$$

Extension to the Case of a Wedge

Use is made of the same calculation given by TOLANSKY, 1948 and BROSSEL, 1947 of the phase-lag of the λ^{th} beam in a wedge interferometer described in Chapter I. So provided the wedge angle and the gap, t are made small enough we can apply the results given above for a parallel plate interferometer to the wedge gap interferometer used in the multiple beam interferometry of surfaces.

Experimental

To observe the effect of varying the reflectivities of the flats on the fringe shape and on the positions of the maxima and minima, Holden used the transmitted fringe system as a reference. To do this, he used a source arm, complete with collimator, which could be moved with respect to a fixed wedge interferometer and viewing system, so that the transmitted and reflected systems could be viewed in turn. Care was taken to see that the collimation was good and that the angle of incidence was small. Mercury green light was used.

The test interferometers were made by evaporating silver onto clean glass flats. Thirteen different reflectivities were deposited on a single flat used for the front surface. The second surface was similarly treated, but with only three

different reflectivities. Scratches were also made on the surfaces to help in comparing the transmitted and reflected systems.

Holden's Experimental Results.

Figure 33, taken from Holden's paper, shows the variation in appearance of the fringes as the reflection coefficient of the first surface varies from 4 to 58%. When the first surface is uncoated glass we have minima coincident with the transmitted maxima. As the reflectivity of the first surface increases, the fringes go through an asymmetrical sequence, until at about 15% the reflected system shows sharp maxima coincident with the maxima of the transmitted system, but much more luminous (the relative times of exposure are 5 : 1). These fringes ($R_1 = 15\%$) were first observed by Hamy.

As the reflectivity of the first surface is increased further, the fringes again become asymmetrical, the background intensity grows, and finally we have symmetrical fringes with fine sharp minima.

It can be seen from the plates corresponding to different back reflectivities that the only effect of increasing the back silvering is to sharpen up all the fringes while they retain their shapes, which are derived only from the front surface conditions. There are in fact two fundamental ways

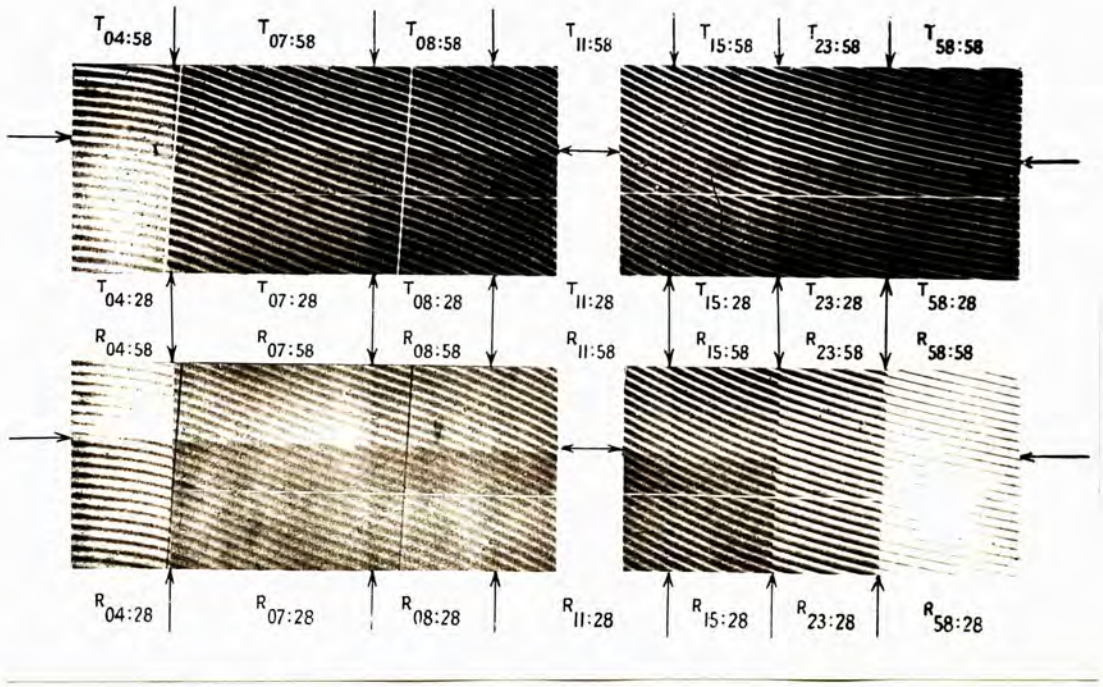
T04:58
T07:58
T08:58
T11:58
T15:58
T23:58
T58:58
T04:28
T07:28
T08:28
T11:28
T15:28
T23:28
T58:28
R04:58
R07:58
R08:58
R11:58
R15:58
R23:58
R58:58
R04:28
R07:28
R08:28
R11:28
R15:28
R23:28
R58:28

Fig. 33.

in which the reflected fringes differ from those seen in transmission. Firstly, the above, that fringe shape depends only upon the front surface properties. Secondly, in transmission the fringe shape is always of the same pattern even when R_1 and R_2 are rather unequal. This can easily be seen by performing the Airy summation for two surfaces and it is,

$$U = t_1 t_2 + t_1 t_2 r_1 r_2 e^{i\delta} + t_1 t_2 r_1^2 r_2^2 e^{2i\delta} + \cdots .$$

$(r_{1,2} = r_1 \text{ etc.})$

As seen above, this is by no means the case for reflection fringes. It may be asked why there is so large a difference between the two systems; the answer lies in the fact that the first beam has suffered no transmission through a reflecting film and only one reflection (at the front surface), whereas the following beams have two transmissions and two reflections - as in the transmitted fringe pattern. Dr. J.A. Belk, of this Laboratory, obtained a transmission-like pattern by cutting out the first beam in a low magnification set-up. In fact, this method has been employed by H. KIMMEL, 1955 for use in measuring film thicknesses. Normally, reflected fringes have to be used, which prohibits the use of a multi-spectrum to identify orders. An aperture was suitably placed in the focal plane of the objective and transmission type fringes obtained. This method cannot be more generally used, as with a non-plane surface the position of the spot in the focal plane corresponding to the first beam is not unique.

Lastly, Holden microphotometered the reflected and transmitted systems and obtained the true fringe profiles using known plate characteristics. By comparison with the transmission fringes the values of Δ satisfying $\frac{\partial I}{\partial \Delta}_{Rx} = 0$ were measured and values of F found from equation 2 . The results are plotted in Fig. 34.

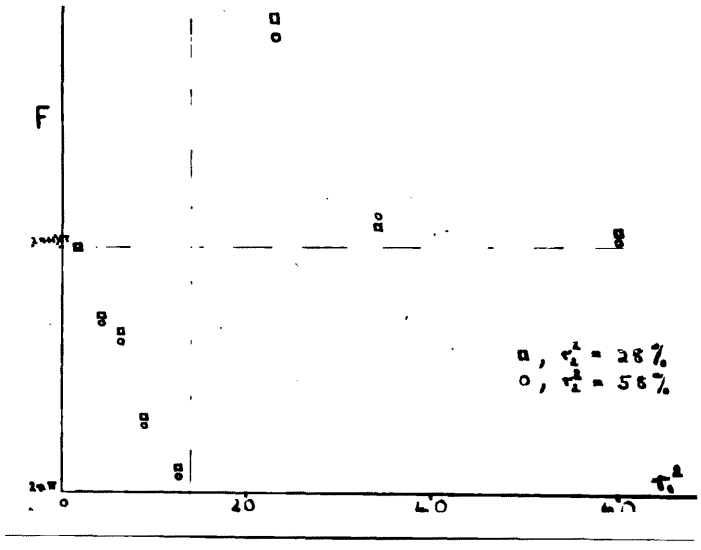

Fig. 34.

The Reflected System at High Reflectivities.

In a very useful section, Holden discusses the case of importance to multiple beam interferometry, i.e., when both films have high reflectivities. Although in this range measurements of F are difficult, it is found that F is nearly $(2m+1)\pi$. The symmetry of the fringes confirms this. (See also FAUST, 1950).

Consider a symmetrical interferometer, we have

$$I_{ax} = R + \left[\frac{T^2 R + 2TR^2 - 2TR\cos\Delta}{1 + R^2 - 2R\cos\Delta} \right]$$

The maxima occur at $\Delta = (2m+1)\pi$ and the minima at $\Delta = 2m\pi$.

The minimum intensity is,

$$I_{min} = R + \frac{RT}{(1-R)^2}\left\{T + 2R - 2\right\}$$

If the films have an absorption A given by

$$R + T + A = 1$$

then,

$$I_{min} = \frac{RA^2}{(1-R)^2}$$

So the effect of absorption is to raise the level of the minima from zero to $\frac{RA^2}{(1-R)^2}$

On the other hand the maximum intensity is

$$I_{max} = R + \frac{TR}{(1+R)^2}\left\{T + 2R + 2\right\}$$

So, for $A^2 \gg 4A$

$$\left[I_{max}\right]^A = \left[I_{max}\right]^0 - \frac{R}{(1+R)^2} \cdot 4A$$

where $\left[I_{max}\right]^0$ is the value when $A = 0$

So we see that the effect of absorption is to

a) raise the minima

and b) lower the maxima of the fringe system.

Thus the contrast of the fringe system is lowered by the absorptive effect.

Holden then gives three really useful graphs. The first showing how the maxima and minima vary with R for, (1) A = 0, (2) A values taken from TOLANSKY'S results for silver films - see Chapter 4 and, (3) & (4), A values two and three times

those for curve (1). The other two plot fringe sharpness against R_1 and contrast against R. (See Figs. 35, 36 and 37).

They illustrate that special care must be taken in order to minimize A - for a given R. Fig. 35 shows clearly that, for a high value of A - curve 3 - the contrast is almost nil at 85%, and quite zero at 90%, while reducing A from 5.5% (curve 1) at R = 90% to 0 (curve o) increases contrast enormously. The other diagrams show the effect of increasing R_1 in the range $\cdot 7 < R < 1$. As R increases the fringe sharpness goes up, but the contrast decreases rapidly. So we have to reach a compromise between sharp and contrasting fringes. Now both these curves depend critically upon absorption. That is they are dependant upon the R-A curves for the particular films we are employing. In Chapter 4 it is seen that these depend in turn rather critically upon the evaporation conditions, e.g. rate of evaporation and hardness of vacuum - and in any given practical case there might be small differences between those actually obtained and the values given later. In principle one should have an accurate knowledge of the R-A curves for the films used and plot (contrast - R) and (sharpness - R) curves and judge which R values give the best compromise between sharpness and contrast. In practice this is not done and good reflection fringes are produced by skill. In any case the overiding factor is to have low absorption films. In this laboratory it is usual to have the first surface, which determines fringe shape, about 60 - 80%, and the back surface, which determines fringe

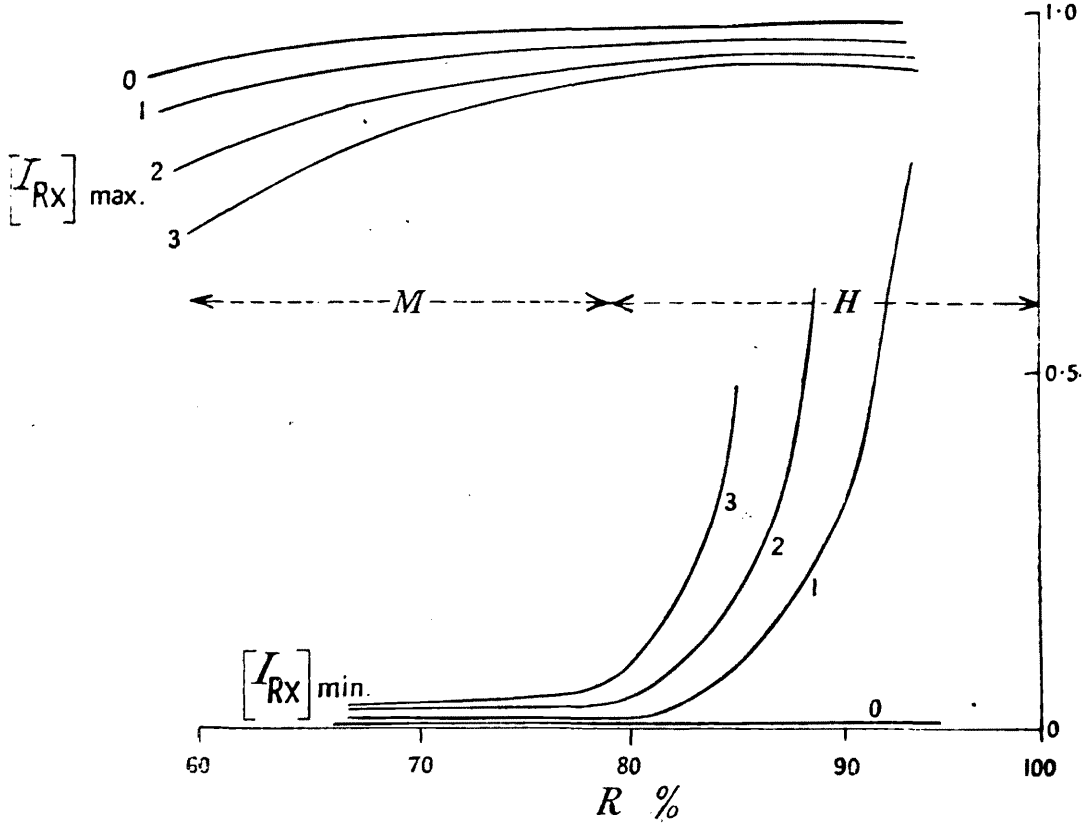

Fig. 35.

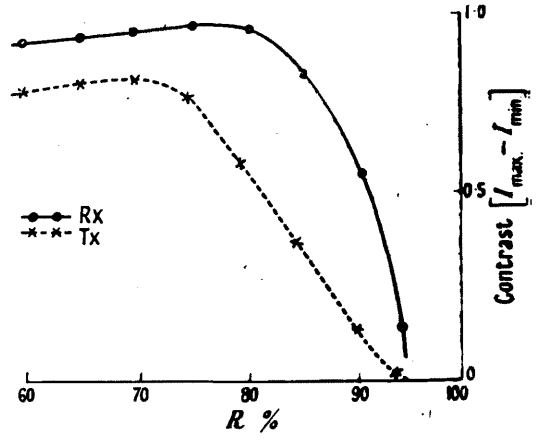

Fig. 36.

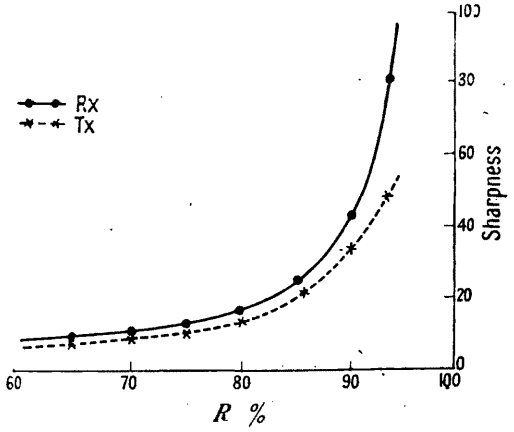

Fig. 37.

brightness about 70 - 90%. Unfortunately, Holden only considered a symmetrical interferometer and a very slight asymmetry is introduced by the use of different coatings, It is common knowledge in this laboratory that, in order to obtain good quality fringes, the back surface reflectivity should be about 10% greater than the front surface. In all events, it is important that the two silverings should be carefully "matched" and that ideal transmission conditions are seldom ideal in reflection.

Asymmetry of the Fringes.

All the precautions discussed in Chapter I to obtain good transmission fringes, such as small values of α, normal incidence, good collimation, etc., have to be taken for reflection work too. In fact all the experimental conditions described in Chapter I, except that regarding the suitable values of R, are applicable here. The vector diagram for the reflection case is shown in Fig. 38 below.

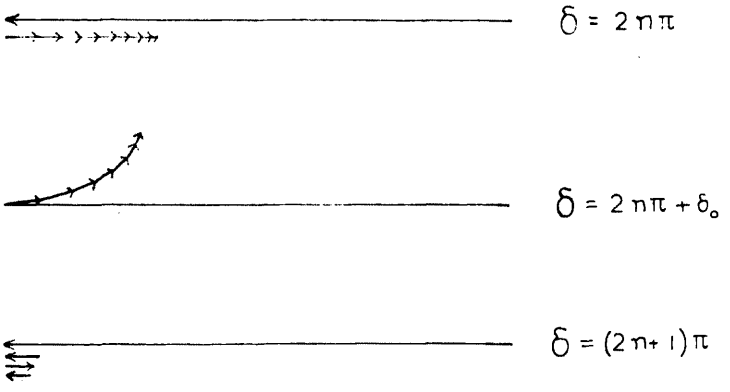

Fig. 38.

However, there is the difference here that any asymmetry or secondary maxima will occur at the edges of the fringes, which are bright. Thus such effects are rather more marked than in transmission. The principle causes of such asymmetry are:-

1. Wedge angle effect (phase lag).
2. Assymetry of the interferometer.
3. Lack of exact focus.

These are not difficult to overcome and with suitable coatings on flat and surface fringes of the quality shown above can be obtained. It will be seen how accurately they contour the surface under test.

This Chapter has extended the fundamental multiple beam Fizeau fringe theory to the important reflection case. The next Chapter will describe how, by combination with a spectrograph, fringes which are more suitable for exact surface measurement can be obtained. Again the theory of the previous chapters applies to a great extent to the discussion of their properties.

CHAPTER III

Fringes of Equal Chromatic Order

When a narrow gap wedge interferometer, as employed for the observation of Fizeau fringes, is illuminated by a parallel beam of white light and the surface imaged by the viewing microscope in the slit plane of a spectrograph, the image plane of the spectrograph is crossed with sharp lines whose shape and separation depends on the shape of the air gap in the interferometer. Thus if the surface under test is matched with a flat, the shape and separation of the lines will give information about the surface topography. These fringes were first described and discussed by TOLANSKY, 1945 (a) and later discussed by TOLANSKY, 1948, who gave them the name "Fringes of Equal Chromatic Order".

These fringes can be used either in transmission or reflection. The optical arrangements in use are shown below in Figs. 39 and 40. As monochromatic light is not being used, care has to be taken over the quality of the lenses employed in the microscope.

In this set-up the wedge behaves as a WAVE-LENGTH FILTER, for, as pointed out in Chapters I and II, the interferometer has high transmission or reflectivity of light when the optical separation of the two plates is an integral number of half-wavelengths. So, for a given gap, only those wavelengths which

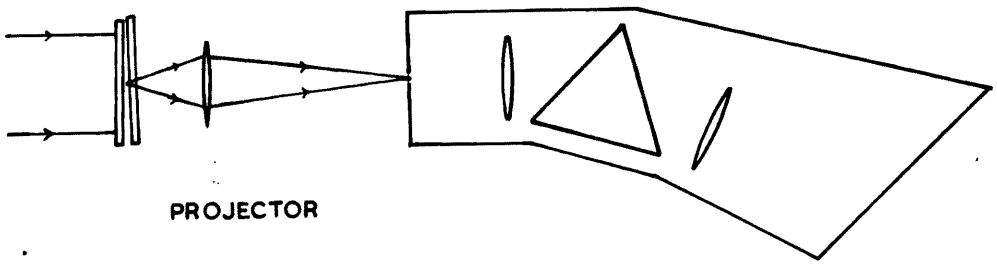

Fig. 39. Transmission F.E.C.O. Set-Up.

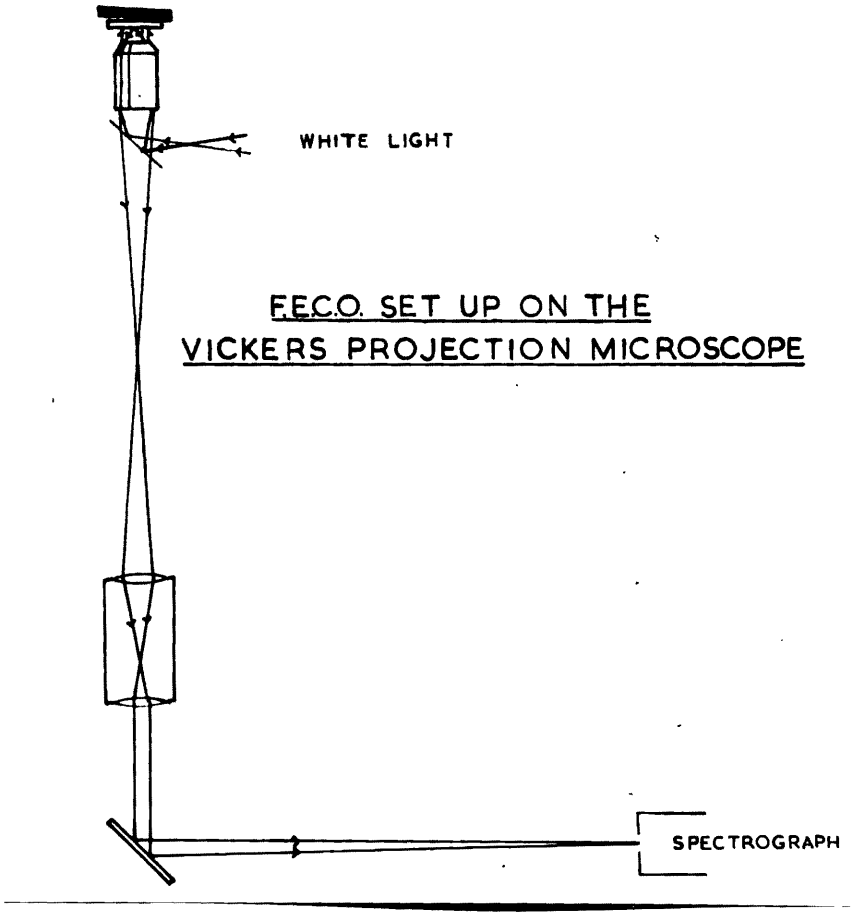

Fig 40. Reflection F.E.C.O. Set-Up.

can fit a whole number of half-wavelengths into the gap, , can be admitted to the spectrograph. It is evident that we are observing the state of interference at the wedge along a line parallel to the spectrograph slit. So any line drawn on the final picture parallel to the dispersion of the spectrograph corresponds to a point on the surface under test. There are in general several fringes crossing the field of view, all similar to one another, and surface structure can be easily inferred by measurements taken along the line drawn parallel to the dispersion.

Two examples of F.E.C.O. are given below. Fig. 41 was taken across a step formed by silvering over a slide already partially silvered in order to find the thickness of the first deposit. It was taken as part of the investigation of Tolansky and Bhide described later. The slit is perpendicular to the step. Fig. 42 was taken across a growth spiral on silicon carbide.

Fig. 41

Fig. 42.

A fringe occurs when

$$m\lambda = 2(t + \varepsilon).$$

where $(t + \varepsilon)$ is the optical separation of the interferometer plates, ε being the contribution from phase changes. So,

$$t = \frac{\lambda}{2}(m - \eta)$$

where is the additional gap due to phase changes expressed as an order fraction of π. η is a slowly varying function of wavelength, but only its <u>variations</u> with λ are of moment when measuring step heights and differences in interferometer gaps - which covers the majority of cases. Except where the greatest accuracy is required, such effects can be ignored. Neglecting variations of η, the wavenumber separation between orders is

$$\Delta\sigma = 1/2t$$

<u>Properties of the Fringes.</u>

Fringes of Equal Chromatic order have several notable advantages over Fizeau fringes. These will now be discussed in turn.

1. Small wedge angles may be used at all magnifications.
   This follows from the formula $\Delta\sigma = 1/2t$

   which shows that the dispersion is independant of α

So α may be reduced as much as possible, with consequent improvement in fringe quality. This is not possible in Fizeau work, where at least three fringes have to be observed at once.

2. Thicker silverings may be employed.

White light sources (e.g. Pointolite) are generally brighter than "monochromatic" sources since no filter is needed and there are no restrictions on source line width. Thus rather greater values of R may be employed with consequent improvement of sharpness of the fringes. This applies specifically to transmission work.

3. In Fizeau M.B.I., it is not easy to determine the order separation of steps and the true direction of the step, i.e. whether it is a rise or a fall. Two spectral lines have to be used and this means, in reflection, two photographs. In the same way, bill or valley questions are not answered straight away. Now, as will be seen below F.E.C.O. gives a definite solution to such problems straight away on one plate.

4. Again, in Fizeau work the dispersion of the fringes is uniform only for a wedge between a pair of planes. In practice, of course, it will vary over the surface under test. In F.E.C.O. the dispersion on the plate is a function of the gap t and the spectrograph only, and we can easily get a profile of the surface along the

projection of the slit on the surface.

Experimental Conditions

The fringe theory in Chapters I and II applies equally well to F.E.C.O. except in so far that the discussion of phase lag effects with respect to numerical aperture is not applicable. The phase lag theory applies, but as values of the wedge angle can be quite small, it is easier to keep the phase term low. In addition to the conditions discussed in Chapters I and II, though, we must consider the effect of the finite spectrograph slit width. The slit cannot be infinitely thin due to loss of light and diffraction effects. So a long thin section of surface is examined instead of a line. The effect depends on the orientation of the wedge w.r.t. the slit. Two extreme cases are considered following TOLANSKY, 1948 and WILCOCK, 1951. There are four causes of fringe broadening in F.E.C.O.

1. Natural line width of the fringes - as discussed in Chapter I.

2. Lack of collimation of the beam at the interferometer - as discussed in Chapter I.

3. Lack of collimation of the beam at the spectrograph prism. This is a fault common to all spectrographs, and is due entirely to the slit width. It results in the spectral lines put on for reference being images of the slit. Provided that diffraction effects in the

spectrograph may be ignored, it is independant of wavelength. As the separation between fringes on the plate generally increases as λ decreases, its effect as an order fraction decreases also as we go from red to violet. This broadening, which has been discussed by VON CITTERT, 1930, occurs even when the wedge apex is perpendicular to the slit.

4. When the wedge apex is parallel to the slit, additional broadening occurs due to small variations in t across the slit projection. That is, it is a defect consequent upon the fact that we are looking at a narrow rectangle of the surface - not a line. This broadening, as an order fraction is $2\sigma\, dt$

Effects 1 and 4 above tend to increase towards the violet, and effects 2 and 3 tend to decrease. By a judicious choice of slope of the wedge apex effects 3 and 4 may be made to compensate increases in each other.

A spurious broadening is sometimes observed due to the greater sensitivity of photographic plates to red radiation, a halation effect taking place.

The fourth broadening effect can be reduced by increasing the microscope magnification. This effectively places a smaller stop in front of the surface. It is almost unique in optics that an increase in magnification is accompanied by an increase in resolution.

Interpretation of the Fringes.

As the spectrograph dispersion is not uniform, the fringes, as seen on the spectrograph plate, are not a true profile of the surface. Differences in height along fringes can be measured as follows.

As, $$m\lambda = 2t$$

$$m\,d\lambda = 2\,dt$$

m is found by measuring wavelengths λ_1 and λ_2 along the line in the plate corresponding to the point under consideration. So

$$m\lambda_1 = (m+1)\lambda_2$$

i.e $$m = \lambda_2 / \lambda_1 - \lambda_2$$

Thus we can find dt from the dispersion curve of the spectrograph.

For a step, the method of coincidences (TOLANSKY, 1948) is convenient. We chose two wavelengths with wavenumber separation $\Delta\sigma$. Let there be m + 1 fringes between these wavelengths on one side of the dividing line and n + 1 on the other. In general m and n are not integers.

Then $$t_1 = m / 2\Delta\sigma$$

and $$t_2 = n / 2\Delta\sigma$$

So $$dt = \frac{1}{2\Delta\sigma}(m - n)$$

KOEHLER, 1953 has considered the case when the variation of η with λ is taken into account. However such precautions are only necessary if an accuracy better than 1 in 1000 .

is required. This can be seen from Koehler's table I. There are two quantities involved in a determination of Δt, a) m and b) $\Delta\lambda$. Now the determination of m involves the use of a wide wavelength range - especially at high dispersions. But m is a SMALL INTEGER and so there is no ambiguity involved by the small changes in η with λ. The determination of $\Delta\lambda$ itself involves only a small wavelength range in general, so errors due to varying η are small. Data on this question has been given by SCHULZ, I95I, KOEHLER, I953, and BARRELL and TEASDALE-BUCKELL, I95I. The latter work is probably the most reliable, having been done for the purpose of high precision wavelength measurements at the N.P.L. Although not with F.E.C.O. in mind, it is readily applicable. Even though the measurements were made using a transmission Fabry-Perot interferometer, the apparent optical thickness, $t+\eta=\frac{\lambda}{2\pi}(\delta+\beta_1+\beta_2)$, in the notation of Chapter 2, is the same in either the transmitted or the reflected system. Using the quantity ϕ given by Barrell and Teasdale-Buckell, the fractional error in Δt is,

$$E = \frac{\phi_1\lambda_1 \sim \phi_2\lambda_2}{m\,\Delta\lambda} = \frac{2(\eta_1 \sim \eta_2)}{m\,\Delta\lambda}$$

$$(\Delta\lambda = \lambda_1 \sim \lambda_2)$$

From (I) above and from Barrell and Teasdale-Buckell's table I we see that E is less in the red than in the blue. This is fortunate as fringe quality improves towards the red end of the spectrum, due to improved quality of silver films at longer wavelengths. It is important to notice that as Δt varies, $\Delta\lambda$ and so $\Delta\eta$, vary in such a way that the fractional error is roughly the same for the working range of Δt values.

CHAPTER IV

Properties of the Reflecting Coating.

It was stated in Chapter I that in order to obtain multiple beam interference fringes the surfaces of the specimen and the flat must be coated with a highly reflecting film which follows the surface structure of the specimen accurately. Three films are used in practise for this work; (a) the well known silver film, (b) aluminium films, and (c) multilayer dieletric films. The efficiency and contouring properties of these films will now be discussed.

The Photometric and Resolution Efficiency of the Transmitted and Reflected Fringe System.

A. Transmission

In Chapter I it was shown that in a transmission Fabry-Perot type system the half-width, as an order fraction is given by

$$\omega = \frac{1-R}{\pi\sqrt{R}}$$

According to BRIGHT, JACKSON, and KUHN 1949, the resolving power $\lambda/d\lambda$ of a Fabry-Perot etalon can be expressed as the product of the order and $1/\omega = \pi\sqrt{R}/1-R$. The quantity $\pi\sqrt{R}/1-R$ is termed the "equivalent number of beams" by analogy with the prism and grating resolving powers. It is customary to plot $N = w^{-1}$ as a measure of the fringe half-width.

We see that N is dependent only R, the reflection coefficient, so to increase N, R must be correspondingly increased. However, the photometric efficiency I/I_o is $T^2/(1-R)^2$ and this decreases with increasing R in the range 0.4 < R < 1 for the three types of film we are considering. The battle between high N and high I/I_o for the three film types will be discussed later.

B. Reflection.

In the reflected system the maximum intensity is no problem - there is generally too much light available instead of too little. More the quantities of interest are the contrast $(I_{max} - I_{min})$, for unit incident intensity, and the fringe half-width, here defined as twice the fractional order when the intensity drops to the value $I_{min} + \frac{1}{2}(I_{max} - I_{min})$. Holden 1949, has discussed the influence of absorption upon these. From the earlier discussion on the reflected system we see that, as the absorption increases, the contrast and the half-width deteriorate rapidly. It is interesting to note that only the absorption of the upper film matters.

Comparision of the Efficiency of Silver, Aluminium, and Multilayer Films.

These three film types will now be compared from the point of view of photometric and resolution efficiency. To achieve these it is evident from the previous section that for a given

R and at a given wavelength, the absorption of the film must be a minimum.

Now multilayer films are designed to work at one wavelength, λ_o, and have unique values of R and A at that wavelength (since the thickness of the layers involved are determined by the wavelength λ_o. On the other hand it is possible to produce silver and aluminium of varying thickness, R and A at any given wavelength. So we have to choose an R, A pair for silver and aluminium films from the available measurements. This choise is complicated by the fact that

(a) in the reflected system, the judgement is made on the basis of high contrast and low fringe width.

(b) in the transmitted system high I/I_o and low fringe width are the guiding factors,

and the dependance of these quantities upon R and A is not the same for (a) and (b). In practice the reflected system is more important, but the contrast and $\frac{1}{2}$-width curves for silver have only been given in the literature for one set of measurements and at one wavelength. They have not been given at all for aluminium. In view of this, and the marked superiority of multilayers oversilver and aluminium from this point of view, since the construction of half-width and contrast curves for the reflection system is very laborious, it has been decided to find representative R A pairs for silver and

aluminium using the I/I_0 and half-width of the transmitted system.

Unfortunately the position is complicated by the fact that the furnished reflectivity and absorption curves for silver differ somewhat. This is an important question, for it is important, from the point of view of obtaining high quality fringes to know the quality of the films which one is depositing. Also, as the quality of the films measured by various authors varies, it is of interest to discuss possible reasons for this.

The Reflectivity and Absorption of Silver Films used in Interferometry.

The early workers in this field were ROMANOWA, ROBZOW, and PROKROWSKY 1934, GOOS 1936, KRAUTKRAMER 1938, and STRONG and GIBBLE 1940. The results of these workers show so much scatter that they are of little use in the region of low A for accurate assessment of performance.

The recent results which will be considered are those TOLANSKY 1946, KUHN and WILSON 1950, and DUFOUR 1951. The results obtained by these workers are shown in Fig. 43.

Fig. 43.

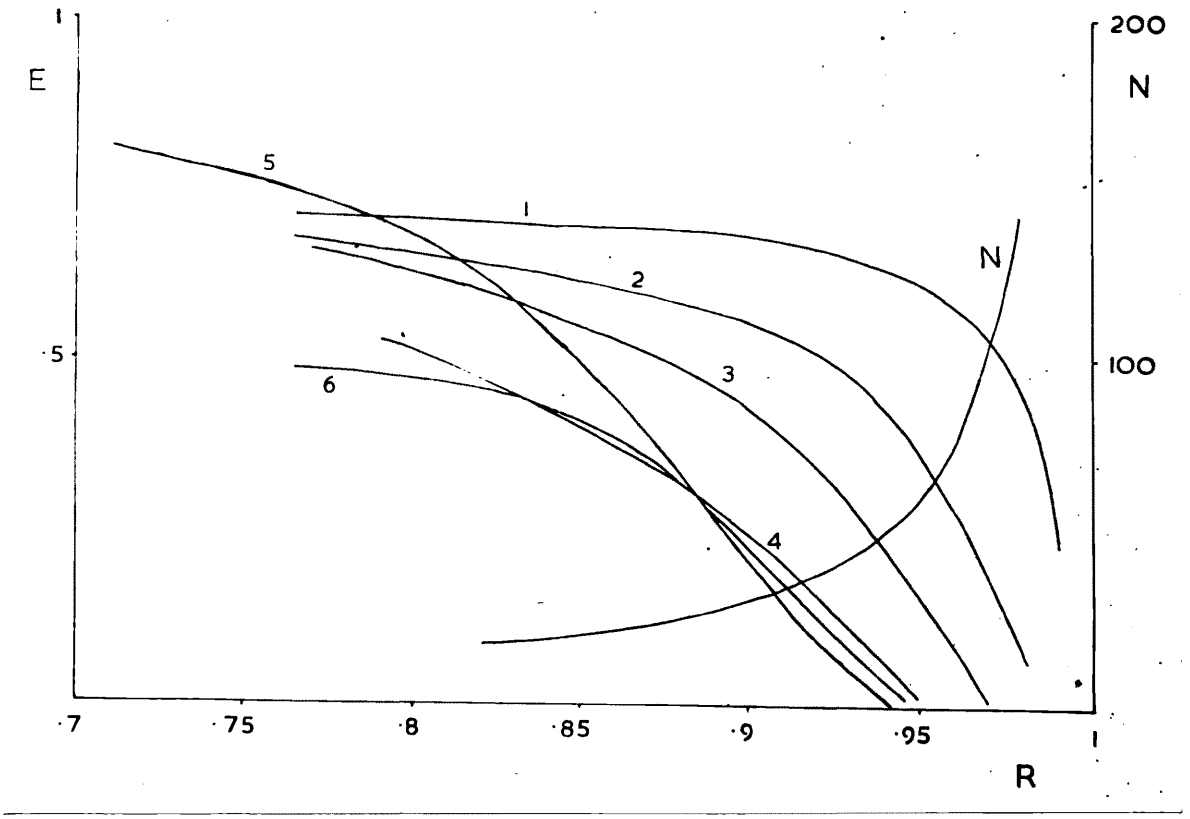

Fig. 43.

Here the quantities $E = T^2/(1-R)^2$ and $N = \pi\sqrt{R}/1-R$ are plotted against R. The film efficiency E is equal to the ratio I/I_0 for the transmitted system, but has wider significance than that, for it is an useful measure of the ratio of absorption to reflectivity. In this figure

curve 1 is taken at 6800 Å, by Kuhn and Wilson (new films).
" 2 " " " 5200 Å. " " " " (" ")
" 3 " " " 4700 Å. " " " " (" ")
" 4 " " " 4200 Å. " " " " (" ")
" 5 " " " 5500 Å. by Tolansky
" 6 " " " 5460 Å. by Dufour

It is unfortunate that these results differ so widely and insufficient experimental data make it difficult to explain the discrepancies, which are greater than the errors quoted for the photometric measurements. It is considered that two effects are to blame, namely varying rate of evaporation and surface films on the substrate. An illuminating paper by SENNETT and SCOTT 1950, indicates that the rate of evaporation plays a big part in determining film quality. They investigated the effect rate of evaporation on the film reflectivities and absorption. Fig. 43 (a) shows clearly the results obtained with films evaporated in 2 sec., 1.5 min, 8 min, 3 min, and 75 min. The symbols ■, ● and ▲ are drawn at reflectivities of 80, 70 and 60%, and the corresponding absorptions are shown in the lower graph. At these three reflectivities the films are in two

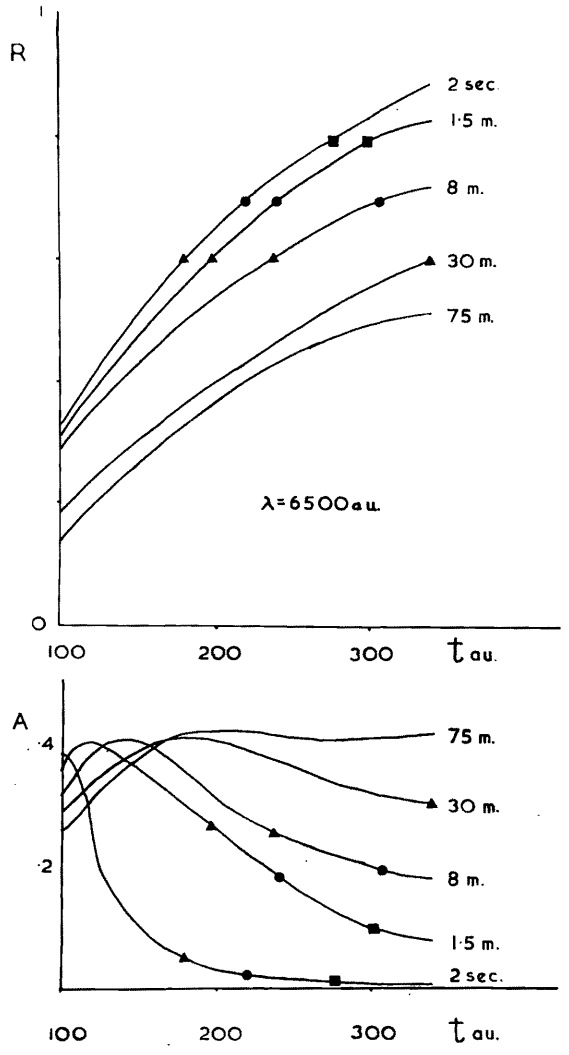
R
1
2 sec.
1·5 m.
8 m.
30 m.
75 m.
λ=6500 a.u.
0
100
200
300
t au.
A
·4
·2
75 m.
30 m.
8 m.
1·5 m.
2 sec.
100
200
300
t au.

Fig. 43a.

groups; low absorption characterized by fast evaporation rates, and high absorption characterized by slow evaporation. Thus high quality films are produced by fast evaporation. It can be seen that the discrepancy in the qualities of fast and slow films is reduced as the reflectivity increases. It is felt though that more information could be obtained about the effect of evaporation rates upon film quality in the region ·٩٨٢١ . This variation in film quality has been attributed by Sennett and Scott to varying grain size in the film. They support this by electron micrographs of their films. On the other hand, BURRIDGE, KUHN and PERY, think that the absorption of gaseous products of the evaporation is largely, or even entirely, responsible. They maintain that while a metal film is being formed, the percentage of foreign atoms occluded in the metal can be expected to depend on the relative rates of bombardment of the surface by foreign gas atoms. If this view is correct, the product of p the foreign gas pressure and τ, the evaporation time, is the factor determining film quality. To test this they plotted the reflectivity curves showing which points had high or low ($p\tau$) values (this was actually done for aluminium films, but the problem is similar for silver). Even with aluminium, which needs more outgassing than silver, no marked dependance of film quality with ($p\tau$) is noticable. It seems rather more likely that grain size is responsible, although occluded gasses may well have a small effect.

The actual cleaning method employed by each of the workers mentioned above will have been different. This is especially true for the high tension gaseous discharge cleaning, about which little is known. The pre-history of the substrate and the air impurities might also have varied. So it is not unlikely that impurity layers, unaffected by the cleaning process, will have produced a systematic effect upon film quality between the results shown above.

Surprisingly the nature of the substrate has little effect upon either grain size or film quality. This has been confirmed by Kuhn abd Wilson and Sennet and Scott. The latter compared films formed on formvar and silica, two widely differing substances while Kuhn and Wilson tested films formed, at the same evaporation, on silica and glass.

It is of interest to note that Kuhn and Wilson measured their reflectivities and absorptions (a) soon after the films were exposed to air and (b) after 22 days in a clean atmosphere. They reported a marked reduction in film quality.

The Reflectivity and absorption of Aluminium Films used in Interferometry.

BURRIDGE, KUHN, and PERY 1953, carried out a series of measurements on evaporated aluminium similar to their previous experiments on silver films. Their results are shown in Fig.44. Aluminium films are inferior to silver films in the region

above 5000 Å., but do not suffer the high absorption of silver films below 4000 Å., and indeed the quality of aluminium increases as the wavelength decreases, as seen from Fig. 44. Representative aluminium films have been taken which have 20 effective beams.

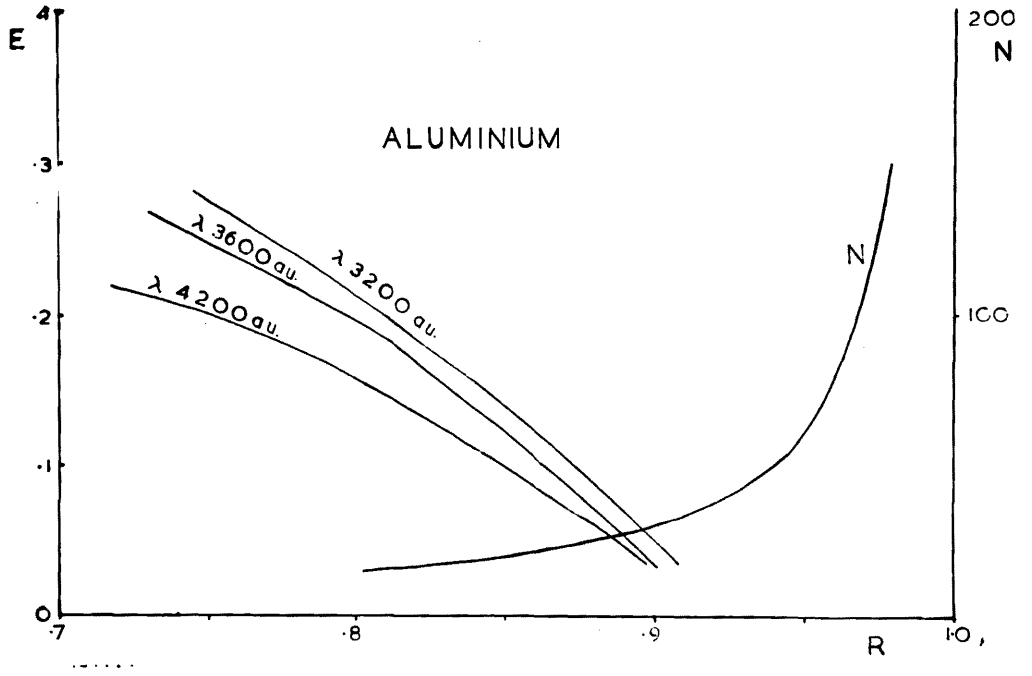

Fig. 44.

Other measurements have been made by CABRERA 1944, and CRAWFORD, GRAY, SCHAWLOW, and KELLY 1949. CABRERA dealt with a wide range of film thicknesses and not with the thick film region in particular. Both Cabrera and Burridge et al. showed that both T and R increase by about 1% within a few hours after exposure to air, but remained steady afterwards in contrast to the rather more unstable silver films. Crawford et. al. showed

the effect of fast and slow evaporation discussed above for silver. However, their results are for a few films only and cannot be compared with those of Burridge, Kuhn and Pery, who measured some hundred films in all. Later measurements by ESSIG and MOLMS (1954) also suffered from this defect.

Multilayer Measurements.

Jacquinot and Dufour were the first to apply the multilayer technique to surface coating in (high resolution) multiple beam interferometry. These highly reflecting multilayers consist of alternate layers of high and low refractive index materials, each having an optical thickness of one quarter the wavelength of the light for which they are designed. (In some cases $3\lambda/4$ layers are used - such coatings are called second-order multilayers). Typical materials used are zinc sulphide (high index) and cryolite (low index) for a glass substrate. The reflectivity depends on the number of layers used; 7, 9 and 11 layers are common for high values of R.

Such highly reflecting films have been produced for interferometric purposes and their reflectivity and absorption measured by JARRETT, 1952 (a & b), 1954, STONE, 1953, RING and WILCOCK, 1953, (in the wavelength region 4000-5000 Å.), BELK, TOLANSKY and TURNBULL, 1954 and by PENSELIN and STENDEL, 1955. The last authors give very extensive results for many types of multilayers and quote results obtained by previous workers. The effects of ageing and rate of evaporation of the materials used

in multilayers have not been studied in so great details as silver and aluminium films. It is well known, however, that multilayers last well for about 2 - 3 months. ROOD, 1949 investigated the ageing of single layers of MgF_2 and $CaSiO_3$ but gives no data about the effect of rate of evaporation. He only considers single films; in a multilayer, the lower layers are well projected. In a later paper he discusses the ageing and effect of rate of evaporation of ZnS films, and comes to the conclusion, like POLSTER, 1952, that rapid evaporation increases absorption (cf. silver). The results of measurements on films designed for use in interferometry are shown in the table below. The representative (RA) pairs for silver and aluminium films are shown for comparison.

The results of the multilayer, silver, and aluminium measurements are shown in Fig. 45. Here the quantity (N.E.), the product of the film efficiency I/I_o and the effective number of beams is taken as a measure of the film's suitability for interferometric work. There is considerable scatter in the multilayer results. This might well be due to effects similar to those resulting in silver and aluminium film quality as well as the difficulties inherent in making multilayer films and in the measurement of R, T and A in the region $\cdot 4 < R < 1$. The multilayers measured were the conventional 9 4 9 layer zinc sulplide - cryolite films, and

No.	λ A.	SYSTEM	R	T	N	E	AUTHOR	SYMBOL	E.N.
1	6200		.967	.027	91	.66	Penselin & Stendel	✕	6.0
2	5800		.972	.019	111	.45	" "	✕	5.0
3	5400		.977	.015	143	.45	" "	✕	6.5
4	5000	$\lambda_0/4$ 9 LAYER	.969	.020	100	.42	" "	✕	4.2
5	4600		.979	.013	143	.37	" "	✕	5.3
6	4200		.978	.012	143	.30	" "	✕	4.27
7	3900	ZnS - CRYOLITE	.981	.012	167	.38	" "	✕	6.4
8	5100		.979	.014	143	.44	Stone	•	6.3
9	5460		.97	.010	100	.11	Jarrett		1.1
10	4500		.960	.032	77	.64	Ring & Wilcock	▲	4.9
11	4300		.958	.030	72	.51	" "	▲	3.7
12	4100		.956	.027	68	.32	" "	▲	2.2
13	5461	$\lambda_0/4$ 7 LAYER	.94	.050	50	.70	Jarrett	▼	3.5
14	5000		.964	.030	83	.71	Penselin & Stendel	■	5.7
15	4600	ZnS CRYOLITE	.955	.035	67	.59	" "	■	3.95
16	3900		.964	.024	83	.43	" "	■	2.7
17	3800	$\lambda_0/4$ - 9 LAYER	.963	.020	83	.29	" "	◘	2.4
18	3600	$PbCl_2 - MgF_2$	.970	.014	100	.22	" "	◘	2.2
19	3400		.959	.017	77	.18	" "	◘	1.4
20	3200	WITH $\frac{\lambda}{2}$ PROTECTING	.979	.012	143	.32	" "	◘	4.6
21	3000	LAYER OF MgF_2	.963	.018	83	.23	" "	◘	1.9
22	6800				50	.625	Kuhn & Wilson	○	3.2
23	5200	SILVER			50	.420	" "	○	2.1
24	4700				50	.210	" "	○	1.05
25	4200				50	.050	" "	○	.25
26	4200				20	.095	Burridge et Al.	○	.190
27	3600	ALUMINIUM			20	.126	" "	○	.252
28	3200				20	.135	" "	○	.270

Results of R and T Measurements Made on Films of Interferometric Quality.

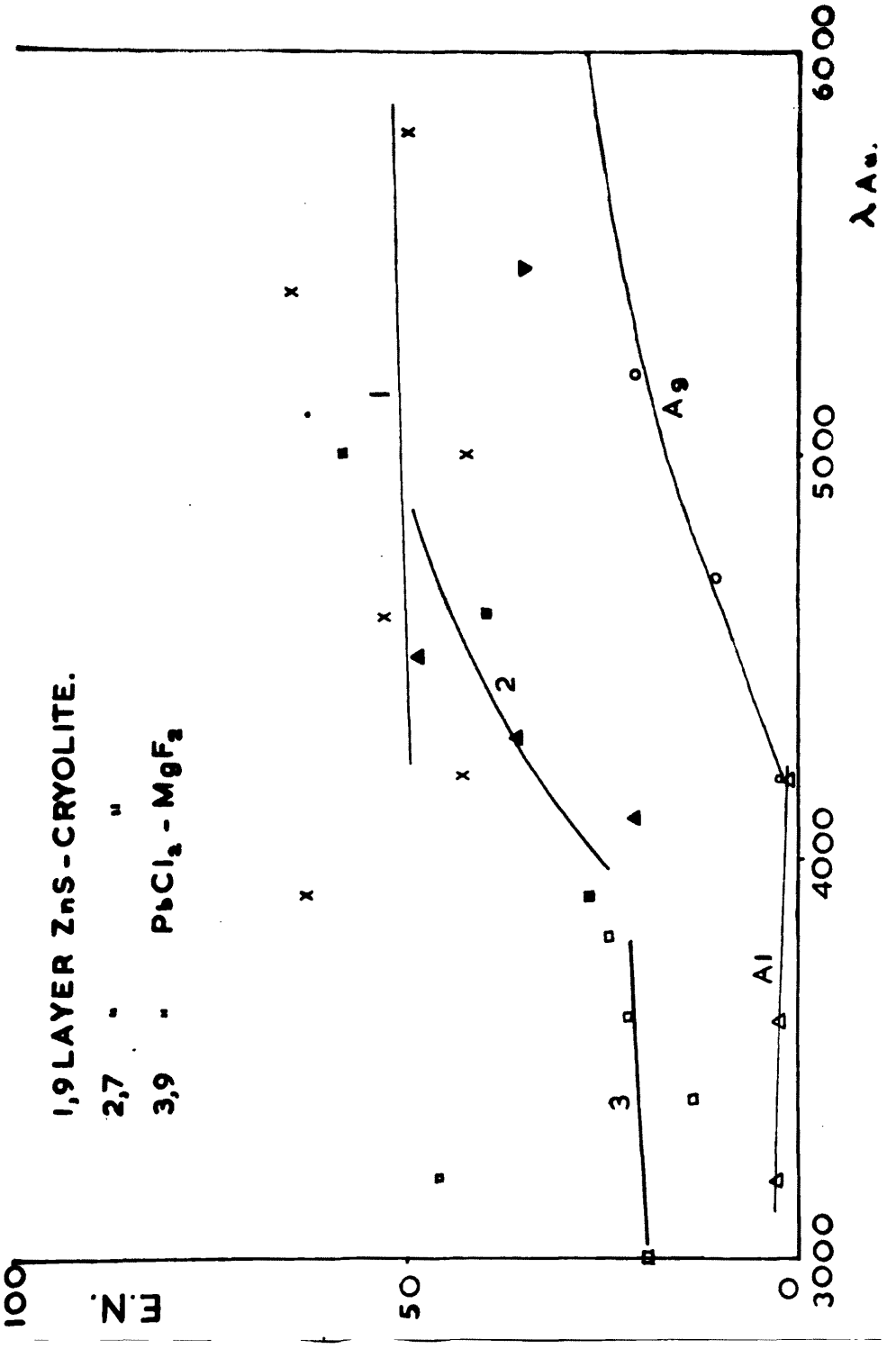
1,9 LAYER ZnS-CRYOLITE.
2,7 " "
3,9 " " $PbCl_2$ - MgF_2
R.N.
100
50
0
3000
4000
5000
6000
λ Å.
Ag
Al
1
2
3

Fig. 45.

the low wavelength lead chloride - magnesium fluoride films produced by Penselin and Stendel (zinc sulphide shows an absorption band at about 4000 Å).

Despite the scatter in the multilayer measurements and the degree of arbitrariness in the choice of points to represent the silver and aluminium films, it is clearly seen that multilayer films have greater efficiency as reflecting coatings in the reflection and transmission Fabry-Perot systems - in short, the graph clearly shows that multilayer films have less absorption for a given reflectivity.

Discussion of the Relative Merits of Silver, Aluminium and Multilayer Films for use in Multiple Beam Interferometry.

The graph shows clearly the superiority of multilayer films over both silver and aluminium in the visible region and ultra-violet. The silver curve rises to only 3.2 at λ 6800 Å ; multilayers in region λ 6500Å. are even higher than this. At lower wavelengths the only metallic film available is Aluminium, due to an absorption band in silver in the ultra-violet at 3000 Å , but gives poor performance films. Unfortunately, the high index material, zinc sulphide, has an absorption band starting at about 4000Å.. An alternative material which has satisfactory U.V. transmission, high refractive index, and good vapourizing characteristics is difficult to find. Penselin and Stendel, in the paper

quoted above, use lead chloride and magnesium fluoirde. Lead chloride is hygroscopic and turns milky in a short time, but they protected the film with a half-wavelength layer of magnesium fluoride. Recently BARR and JENKINS 1956, have tried films using antimony trioxide, and preliminary results show promise. This question is of importance, as it is the U.V. that high metrical accuracy is obtained using multiple beam interferometry (since λ_2 here is less in centimetres than λ_2 in green light), and the available metallic films are of rather poor quality.

Kuhn and Wilson 1956, remeasured their silver films after keeping them in moderately clean air for 22 days. They found a reduction of film efficiency due probably to formation of the sulphide. Aluminium films do not suffer so much deterioration, and this all occurs within a few hours after exposure to air, Multilayers, on the other hand, show little deterioration even after several months, a fact which is well known in this laboratory.

One of the properties of multilayer films is their chromatic filtering action. Their operation depends upon an interference effect so this might be expected. The pass band for the quantity $r^2/(1-r)^2$ is often only of the order of tens of Angstrom units - see, for example, STONE 1953. Consequently, a multilayer film should only be used for the wavelength for which it is designed (i.e. at that for which

the optical film thickness is $\lambda/4$). For Fizeau work this is no defect, as monochromatic light is used, but it means that multilayer films cannot be used for fringes of equal chromatic order. If a channelled spectrum is obtained using multilayers, the fringes broaden out considerably on either side of the wavelength at which the reflection maxima occurs. This property has been used by BELK, TOLANSKY, and TURNBULL, 1954, in the examination of surfaces by reflection Fizeau fringes. They used a second order multilayer giving maximum reflection at 5460 A., and formed the fringes using this wavelength. They then used a red filtered carbon-arc in the microscope. Since for this wavelength the film transmits about 90% of the incident light, the surface could be viewed directly. In this way the actual surface and its interferogram could be directly compared.

The efficiency of a multilayer film depends upon the refractive index of the substrate, as well as the layer constituents. Multilayers have been successfully deposited upon glass or quartz, but to produce efficient multilayers upon any given material is difficult. Not only is it difficult to do this, but there is considerable danger of artefact in the fringe pattern. This might arise in the following way. In a silver film, 300 A. thick say, the front of the film contours the topography under examination. The reflections produced by the silver effectively take place at

a surface parallel to the front silver surface, a short distance within the silver. This surface is well defined, unique, and parallel to the surface under examination. But however well a multilayer will contour a surface, the various reflections will take place at 7, 9 or 11 different levels each $\lambda/4$ (i.e. 500 to 700 Å.), apart. So we see that there is likely to be a danger of artefacts at large wedge angles and for sharp or rough surfaces.

The situation is not as bad as might seem, for in reflection Fizeau work, which is the most important in which multilayers are employed, the usual practise is to coat the surface under examination with a very thick coating of silver. Then only the properties of the film on the flat determine the fringe quality. We can so use multilayer films to advantage on the optical flat. Their long life makes them particularly useful here. (However, in this case the difference in R between the flat and the surface produces a slight asymmetry in the fringes. To obtain fringes of the highest quality both surfaces have to be coated with identical films). Further articles dealing with the use of multilayers in multiple beam interferometry have been published by TOLANSKY, 1952 and TURNBULL and BELK, 1952.

It is a fundamental assumption in the examination of surface topography by multiple beam interferometry that the reflecting layers shall contour the surface closely. There

is much indirect evidence that surfaces are well contoured by silver and multilayers alike. For example, mica cleavage steps have been measured by multiple beam interferometry and in all cases have been found to be multiples of 26 A. , which is the size of the mica lattice spacing, as obtained from X-ray determinations. Also interference filters formed by deposition of the system (silver - cryolite - silver) on glass give quite narrow transmission bands, even though quite irregular substrates are used. Direct evidence on this problem has been given by a recent paper by TOLANSKY and BHIDE (private communication). They took a silicon carbide crystal which had well defined spiral pattern. It was examined by reflection eclectron microscopy and the step shown to be quite sharp. Silver was evaporated onto the crystal in varying thicknesses from 250 to 26,700 A. . This thickness was measured by evaporating, at the same time, the silver onto a glass plate covered with an opaque silvering. The measurement was then made using reflection F.E.C.O. The apparent step height was measured, also by F.E.C.O., (a) at the step itself, and (b) .06 mm. from the step. The results are shown in Fig. 46.

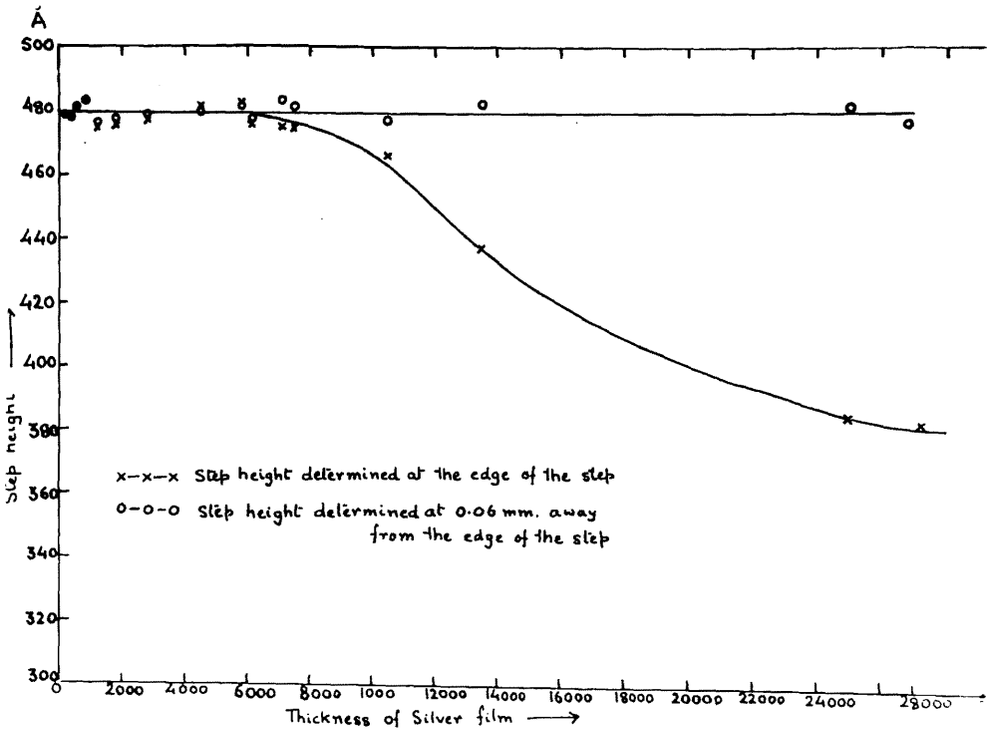

Fig. 46

This shows that :-

a) Up to a silver thickness of 6000 Å . the contouring is perfect even at the edge itself.

b) Up to 28,000 Å contouring is perfect at distances beyond 1/15 m.m. from the edge.

c) For any thickness beyond 6000 Å a defect begins to appear in the step height measured at the edge and it increases to about 100 Å. at the max. film thickness of 26,700 Å..

Since in multiple beam interferometry the thickest

films are of the order of 1000 A. thick, these experiments confirm that we may rely upon silver films to contour details upon surfaces examined by multiple beam interferometry.

Tolansky and Bhide also performed similar experiments upon zinc sulphide and cryolite films. Even though multi-layers are not usually used to coat surfaces under examination to obtain really sharp contrasting reflection fringes it is preferable to have both surfaces with exactly the same value of R . For this reason Tolansky and Bhide considered it worth while investigating zinc sulphide and cryolite contouring.

The same step on silicon carbide was used as before and the measurements were made as for silver. The results are shown in Fig. 47 for zinc sulphide.

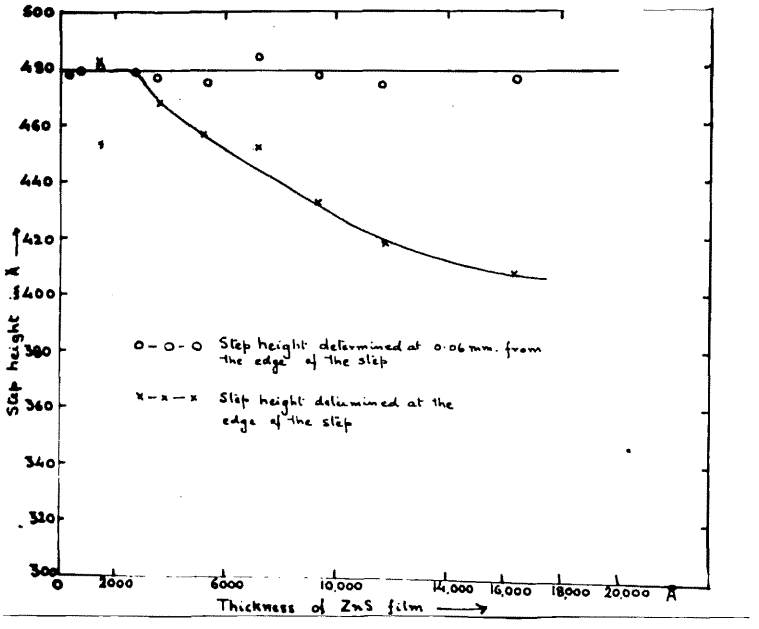

Fig. 47.

We see that for zinc sulphide, contouring is perfect at the step up to a thickness of about 2000 Å of zinc sulphide. Beyond .06 m.m. from the step edge contouring is perfect at all thicknesses.

Similarly for cryolite, we find that contouring is

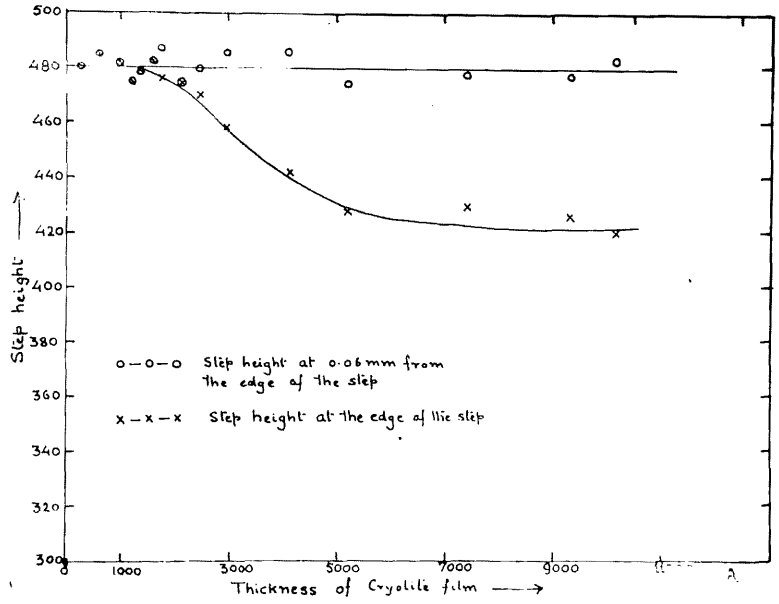

Fig. 48.

perfect up to film thicknesses of about 1000 Å. . This is of the same order as the metrical thickness of a quarter-wave film at 5460 Å. . Again beyond .06 m.m. from the step contouring is perfect even at great thicknesses, but nearer the step there is a pile up of cryolite at the step when the film deposited is thicker than about 1000 Å. .

Tolansky and Bhide's results show that we may rely upon silver contouring in multiple beam interferometry as the film thicknesses are seldom more than 1000 Å . On the other hand, care has to be taken when using multilayers to contour small structures. These films generally have .9 layers in all, 5 of ZnS and 4 of cryolite. The metrical thickness of $\lambda/4$ of cryolite at 5400 Å is 1000 Å . . So we will have 4000 Å. of cryolite in all. This is beyond the safe limit of 2000 Å. . In fact the cryolite is in four distinct layers, and we might expect the effect to be less than on a single film 4000 Å. thick. Tolansky and Bhide carried out an experiment with silver by depositing 6000 in 6 separate evaporations, upon the silicon carbide step and found the step defect to be less than for 6000 Å. deposited in a single evaporation. Nevertheless, the danger of lack of contouring of small structures with multilayers still exists

To sum up, the results of many reflectivity and absorption measurements on silver, aluminium and multilayer films (displayed in Fig 45) shows clearly the superiority of multilayers over both silver and aluminium films from the point of view of fringe intensity and sharpness. This is especially true of the ultra-violet region, but holds to a lesser extent at much greater wavelengths. Multilayers have the further advantage of good keeping qualities; a film, although rather more difficult to make than a simple silver deposition, will last for several months. On the other

hand, their quality has a marked dependance upon wavelength with the result that they are unsuitable for F.E.C.O. work. Furthermore, they can only be deposited easily upon a glass substrate and even then their contouring properties are in doubt for small objects. These last objections, however, are only relevant in reflection work, if we are striving for fringes of the very highest quality; usually the back surface (that under examination) is coated with a thick silvering. In short, multilayers are eminently suitable for use on the optical flats used in reflection Fizeau multiple beam interferometry, but are unfortunately not available for F.E.C.O. as yet, although a recent paper (BAUMEISTER and STONE, 1956) describes a multilayer film of exceptionally wide band-width in which the layers were not of the usual $\lambda/4$ and $3\lambda/4$ type, but were calculated by a matrix method using a I.B.M. card catalogued computer.

Appendix to Section 1.

Experimental Techniques.

The principles of the multiple beam interferometry of surfaces having been given in the previous chapters, some of the experimental techniques employed, in this laboratory, in its practise are described below.

Before evaporating silver, aluminium, or a multilayer onto a test surface or a flat, it has to be very thoroughly cleaned, otherwise the film will not adhere or will be of poor quality. The cleaning process used depends, of course, on the nature of the surface material; care has to be taken that cleaning reagents do not attack the surface in any way. Glass, diamond, silicon carbide, and other highly resistant materials are generally cleaned (see TOLANSKY, 1948 and STRONG, 1946) by a preliminary washing with teepol and water followed by rinsing with caustic soda, water, and then nitric acid. The final cleaning is effected by leaving over-night in hydrogen peroxide and then rubbing with cotton wool soaked in hydrogen peroxide until clean. The surfaces are judged to be clean when, upon rather heavily breathing on the surface, the condensation appears to be absolutely uniform. This test is best carried out by holding the specimen at about eye level in front of a window and viewing the surface at an angle of 20-30°. Metallic surfaces have to be treated with more respect. In many cases they are not

silvered, but have a natural high reflectivity after polishing. Otherwise, TOLANSKY, 1948 has recommended that they be degreased with ethylene trichloride. The ethylene trichloride is gently boiled in a beaker closed with a watch-glass. The specimen is suspended above the liquid, the vapour condenses on the surface, degreases it and the impure liquid drops back. In all cases, the final cleaning is by ionic bombardment in the evaporating vessel.

The technique of thin film evaporation has been described by TOLANSKY, 1947 and 1948, STRONG, 1946, LEWIS, 1946, and HEAVENS, 1954. In this laboratory, an Edwards standard evaporating plant, type E3 is used. This is of the vertical type, the chamber being a pyrex bell-jar, 60cm. high, resting on a massive steel base-plate. The vacuum seal is a rubber L - gasket on the lower rim of the bell-jar. A number of insulated electrodes pass through vacuum seals into the chamber. Two of these are connected to flat rings fitting just inside the bell-jar. An a.c. potential of 3,500 v. is applied between these when the pressure falls below .5 m.m. of Hg. and the specimens receive their final cleaning before evaporation. The specimens are mounted face downwards about 30cm. above the filament. A large glass disc above the specimen holder prevents the top of the bell-jar from becoming coated with silver. The silver, in capsule form, is placed in a small depression in a molybdenum strip,

which acts as the filament. A baffle is placed just above the filament - this is mounted on a vertical rod to enable it to be removed when actually evaporating. All the mountings, etc., in the plant are of aluminium, to reduce sputtering. A current of about 90 to 120 amps is passed when evaporating. When the vacuum in the chamber is better than 10^{-4} m.m. of Hg a heavy current (150 amp.) is passed to degas the silver. This is reduced to about 90 amp. and the baffle removed until a sufficiently thick film has been deposited. This is judged either by viewing the films from above, or by timing. The vacuum which must be reached before starting the evaporating is determined by the distance from the filament to the specimen. This must be much less than the mean free path of the silver atoms, On the other hand, the specimen - filament distance must be large enough to secure adequate uniformity of coating, (this is helped by the fact that the molten silver is not a point source but has an effective radius of $\frac{1}{4}$ - $\frac{1}{2}$ cm).

The reflectivity of the silver films may be estimated by eye, after experience, due to the differential absorption of silver to blue and red light. A thick silvering will appear deep blue when held towards a window. An alternative method of quick evaluation is the observation of a pea bulb through two films having a small angle between each other. The number of images of the bulb seen gives an idea of the quality of the film after experience. For more accurate

work, a Strong instrument may be used.

The production of multilayer films is carried out, quite successfully, in this laboratory as follows (see BELK , 1954). ZnS - cryolite films are generally used. Two filaments, which are "boats" of molybdenum, are used side by side with a glass sheet in between to prevent contamination of one by the other. The important feature is the method of thickness control used. This is the one originated by BANNING, 1947. The control is effected by visual observation of the change of colour of the light reflected from the films. As the thickness of the film increases the wavelength for which the film has its maximum reflectivity changes and so the colour of the reflected light changes. The table below, given by Belk, lists the colour of light reflected by the films from a 60 watt opal bulb for various thicknesses (in green light).

Colour		Optical thickness for Green Light
ZnS	Cryolite	
Blue-white	yellow	
white	magneta	$\lambda/4$
yellow	blue	
magneta	white	$\lambda/2$
blue	yellow	
Greenish-white	magneta	$3\lambda/4$
yellow	blue	
magneta	greenish-white	λ

A monitor is used to judge the thickness of different layers. It can be partially or wholly covered by a movable baffle, similar to that used in the silvering plant, and a fresh section is exposed for each successive layer. For more accurate work a photoelectric method may be used.

The interferometer set up and used in this laboratory is generally a jig, consisting of two annular plates held together by spring loaded thumb screws - see Fig. 49. The flat - which is usually a piece of ordinary cover-glass (these are generally plane enough over small regions) is held against the specimen by the plates. To examine small regions in a convex portion of a specimen a micro-flat is used. This is a small truncated cone of glass with plane-parallel ends about 4 mm. thick, the wide end being about 5 mm. in diameter and the thin end less than 1 mm. It is made by cutting a small cylinder out of a small glass flat and mounting on a rod, the ends being coated with wax for protection. The cylinder is then ground down to a cone with a carborundum wheel.

Fig. 49.

Lastly, most of the work here is done using the Vickers Projection Microscope. This has the advantage that the specimem is above the objective. Also it is easily set up for Fizeau or F.E.C.O. work and plates can be taken readily.

PART A

SECTION II

Two Beam Interference Microscopy.

Two Beam Interference Microscopy.

Interference microscopy has come into being on account of shortcomings in two other optical methods designed to study surface microtopography, namely, multiple beam interferometry and reflection phase microscopy. It of course has its own shortcomings, but provides an extremely useful tool in its own province, the study of microstructures of surfaces at high magnification. Owing to the very nature of phase microscopy it detects only more or less abrupt changes in surface height and can tell us nothing about the more gradual variations of surfaces. A further snag of the phase-contrast microscope lies in the well known halation effect. Due to the finite stop introduced by the annular ring of the phase plate an object, intended to appear dark, is surrounded by a bright band. This effect is of small moment in biological work, where small unstained refractile bodies are made visible, but can be highly confusing in the more extensive structures generally observed on opaque surfaces. In addition, a normal phase microscope is primarily of use for the detection of small structures and if these are appreciably greater than $\lambda/10$ in height phase contrast offers little advantage. Quantitative work with the phase microscope is a matter of estimation rather than of accurate measurement. As explained earlier one of the drawbacks of multiple beam interferometry is that its use at high magnifications is limited by the third order correction

term ($4/3\ h^3\alpha^2\ k$) to one or two fringes near to zero order.

The two beam interference microscope improves on this somewhat and orders of interference up to about five, even at x 1000 can be employed. Here the maximum order is governed by the depth of focus of the microscope. Thus it decreases as the magnification goes up, but is still rather larger than permissible with say, a 4 m.m. objective using multiple beam Fizeau fringes. The important feature of these instruments is that the reference flat is a virtual image of a plane silvered surface. Thus one is not restricted to the "tops" of microstructures by the necessity of having extremely thin air films between the surface and a solid flat. It is true that the surface will only be contoured accurately in the region of low orders (why this is so will be explained later) but low order interference is always obtained in the region where the objective is focussed. For example, if we are examining a steel ball bearing surface, the use of the solid flat restricts observations at high magnifications to a few orders at the crown; by using a virtual flat, we can focus further down on the sides of the bearing and still obtain low orders. In addition, fringes on both sides of zero order can be seen, which doubles the range of height observed for a given depth of focus. However much vertical resolution is lost by employing the two beam fringes with their cosine squared distribution of intensity. This is a serious

drawback to the use of this instrument and explains why it is preferable to use multiple beam fringes if possible. Recently multiple beam fringes have been employed successfully at high magnifications on a diamond surface, (TOLANSKY and EMARA, 1955).

Having explained the raison d'etre of the two-beam interference microscope, the optical systems used will now be explained. The basic principle behind all such instruments is that a virtual image of a plane reference surface is brought near to the surface under test. Both the image and the surface are viewed by the normal convergent microscopic illumination, either by the same or by different, matched, objectives. The wavefronts reflected by the image and the surface interfere showing up the surface contouring in a two beam pattern. The optics of such a system is rather different from the Fizeau set-up in that critical illumination is used instead of Köhler illumination. The two spherical wavefronts diverging from a point on the surface and a corresponding point on the flat interfere to give fringes in the image plane of the objective. These two points have to be within the depth of focus of the objective.

The three practical set-ups that have been published for use in micro-interferometers will now be described.

The Linnik System

This is the earliest two-beam microscope interferometer to be described. It is an instrument related to the

Michelson interferometer and was first used by LINNIK in 1933 (see LINNIK, 1933). The parallel beams of the Michelson set-up are focused onto the surface under test (M_1) and the reference flat (M_2) by two matched objectives, L_1 and L_2. The surfaces are observed by the eyepiece L_4. The image of M_2 is adjusted to be close to M_1. Two beam fringes contouring M_1 are then seen through L_4. In the path beam AL_2 is a plate, the tilting of which enables the fringe dispersion and position to be modified at will. (See also Rantzch, 1945).

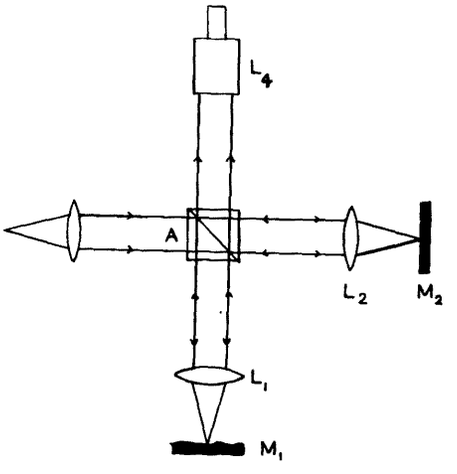

Fig.1.

This instrument requires a very robust construction and is sensitive to vibrations and temperature effects. It requires a pair of carefully matched objectives for efficient operation. In 1954, GRUBE and ROUZE published

a paper showing several interferograms taken with a Linnik instrument.

A modern microinterferometer similar to the Linnik instrument has been described by PERRY, 1955. As shown in Fig. 2 the two beams are not collimated, but are directly focused onto the surface and flat by the two matched objectives.

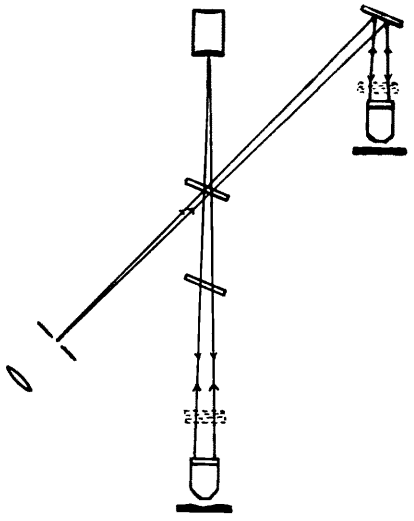

Fig. 2.

The thickness of the beam splitter and compensator have been kept to sufficiently low values to avoid even order defects which they might introduce into the objective optics. It uses 4 m.m. and 16 m.m. objectives, giving magnifications ranging from 78 to 750 times. To give uniformity of fringe visibility with varying specimen surface finish, the flat is

mounted eccentrically and is metallized in two adjacent 120° sectors giving reflection coefficients of approximately 95 and 40 per cent, the third sector being left immetallized. An adjustable wedge compensator situated just above the lower objective, together with its counterpart in the other beam provides a fine adjustment of the path difference between the two beams.

The Mirau System

This system (DELAUNAY, 1953) employs only one objective. The virtual image of the flat, which is merely a silvered portion of the objective front face, (see Fig.3) is produced by the beam splitter P_1, P_2.

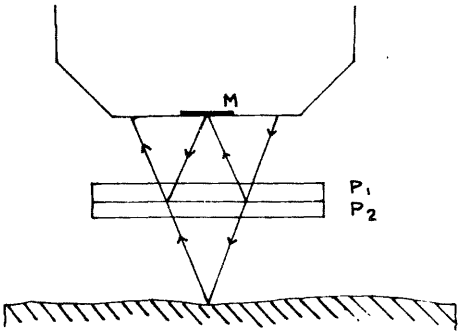

Fig. 3.

The snag with this arrangement is that it requires a rather large working distance to the objective and that the aperture of the objective is cut down somewhat by the "flat".

The Dyson System

A rather more elaborate arrangement employing a single objective, but which has no restrictions as to working distance, was first described by DYSON in 1953. This is somewhat different to his transmission instrument. The optical system is shown below in Fig. 4.

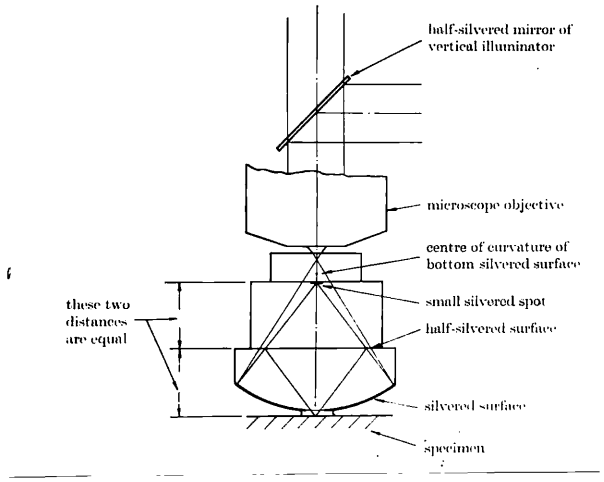

Fig. 4.

A system of three blocks, of high optical quality, cemented together, is placed below the objective. The lowest block has a plano-convex shape, with the plane surface uppermost. The top surface is half-silvered and the bottom one has an opaque coating save for a small region near its

pole. The middle block is plane - parallel and bears a small silvered spot on its upper surface, to which the top block is cemented. The thickness of the lowest block is slightly less than half the radius of the convex surface and that of the middle block is such that the radius of curvature of the convex surfaces is about a millimeter above the silvered spot.

The convex surface is then oil-immersed onto the specimen in such a position that the specimen and the silvered spot are equidistant from the half-silvered surface. Images of surface and flat are then formed just above the centre of curvature of the convex surface. Two beam fringes are formed between these two images. Illumination is by the conventional vertical illuminator.

In order to give a fine adjustment to the separation between flat and surface the arrangement shown in simplified form in Fig. 5 is used.

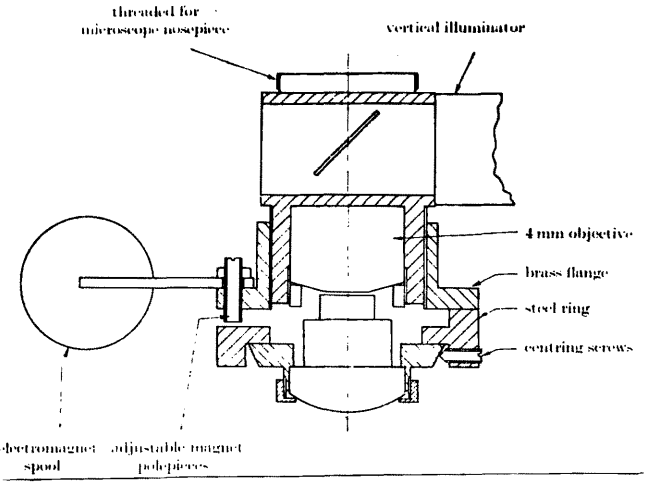

Fig. 5.

The relative positions of the objective and interferometer is adjusted by the dectromagnet. Very fine fringe displacements can be obtained using this devise.

Having described above the three types of interference microscope in use, we will now discuss the general properties of the system. These have been discussed in detail in a paper "Interference Microscopy at High Wedge Angles" by MYKURA, 1954.

The Vertical Range of the Instrument

The vertical range of the instrument is limited by the optics of the illuminating system and of the viewing system. In reflection, of course, these are the same, but their effects on the vertical resolution are rather different. In order to obtain interference between the wavefronts reflected from the flat and the surface, the illumination of the corresponding points on these two surfaces must be coherent. To be more precise, the coherent illumination at the two points must have approximately the same amplitude. So, intuitively, the two points must be within the depth of focus of the condensing lens of the system, which is the objective in this case of course. Dyson, in an earlier paper on his transmission instrument (Dyson, 1950) calculates the visibility of the fringes as a function of the separation of the corresponding points on surface and flat giving,

$$V = \frac{J_1(2\pi d n \sin \alpha/\lambda)}{\pi d n \sin \alpha/\lambda}$$

Here d is the separation of the points in a direction parallel to the axis and α is the semi-angle of the illuminating cone. This expression is .808 of its maximum when $2\pi d \sin\frac{\alpha}{\lambda} = 1$, so we see that fringes of quite appreciable visibility will be obtained even when d is rather larger than the depth of focus.

The viewing optics, however, are effected in a rather different way. When the reference plane is in focus the ray optics are shown in Fig. 6.

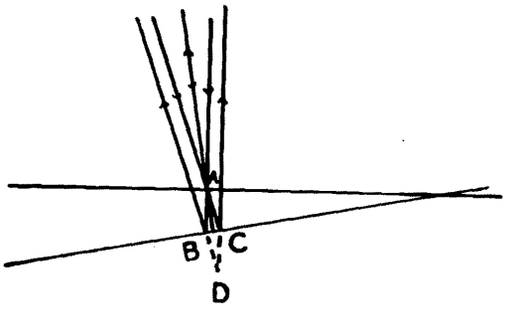

Fig. 6.

Outside the depth of focus, the light coming from the surface is reflected from a region BC. Thus a true picture of the surface will not be given unless it is within the depth of focus of the objective. Nykura gives a very good illustration of this in his paper. He shows a portion of an interferogram of a 1 mm. steel ball with scratches taken

on a Zeiss-Linnik interferometer. It shows clearly how the fringes only contour the surface accurately near the zero order fringe. Outside this depth of focus region of about five fringes on either side of zero-order we see that there are fringes, but of diminishing visibility, as explained above. This reduction in visibility is complicated by the varying wedge angle as explained below.

Variation of Visibility with Wedge Angle

As can be seen from Fig. 6 , the cone of lights from the surface and the flat are not coaxial, the angle between their axes increasing with increasing wedge angle. Correspondingly, the light flux entering the microscope from the surface will vary with wedge angle and with it, the visibility of the fringes. Nykura pointed this out and plotted visibility against wedge angle - see Fig. 7.

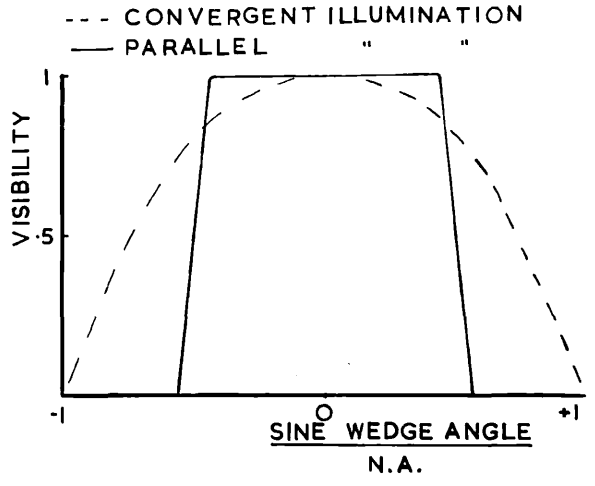

Fig. 7.

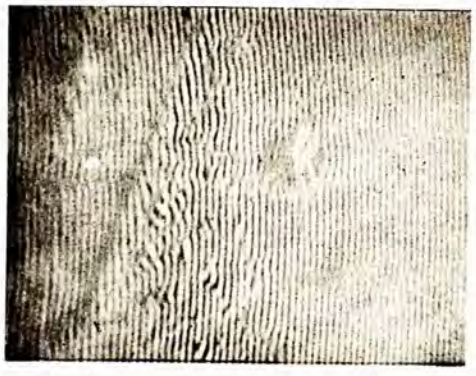

Two-beam interferogram taken on a Zeiss-Linnik instrument, as given by Mykura. Note how the fringes only contour the surface near the zero order fringe.

It will be seen that the maximum wedge angle giving fringes of reasonable quality is rather less than the semi-angle . The corresponding quantity for two beam Fizeau fringes is shown.

To sum up, three arrangements which permit two beam fringes to be observed between a surface under test and a flat, using critical illumination, have been described. The continued use of critical illumination and two beam fringes enables higher magnifications to be employed than is usual with multiple beam Fizeau fringes. The range of surface structures which can be observed by this method is limited by the finite depth of focus of the objective to a few orders, but, having a virtual flat, we can focus "down the specimen". On the other hand the fringes have only the broad $\cos.^2$ distribution, so the vertical and angular resolution is very poor. Lukura gives about 5 to 10% for the accuracy of angle measurement between 30° and 10°. Really accurate mapping of surface micro-topography is impossible and the very small details seen on the surface at high magnifications merely blur and confuse the fringes. Pictures of surfaces with a lot of detail do not come out at all well with two beam fringes, and in fact look messy, especially when compared with the corresponding multiple beam picture.

SECTION III

Surface Profile and Shadow Casting Microscopy.

The Surface Profile Microscope

In 1952 TOLANSKY, 1952 (b, c and d) described an improved version of the SCHMALTZ (1936) light-cut technique. The Schmaltz method used one objective to focus the image of a fine slit onto the surface, the illumination being at 45° to the normal. The surface, thus illuminated, was viewed by another objective at 90° to the first. In this way the variations in surface height are revealed as lateral shifts of the image of the slit. The original Schmaltz method could only be used with large working distance objectives (i.e. at low powers) as the two lenses approach each other at 45°. This objection was overcome by various workers, but only at the expense of the objective aperture, and hence resolution. In any case, light cut methods have the disadvantages that they have a "chopped" appearance due to regions of non-specular reflection, scattered light leads to image broadening, the whole surface cannot be seen at the same time as the light cut, and only one profile line appears.

The light-profile technique overcomes all these difficulties and provides a simple and accurate method of measuring surface features down to $\lambda/2$ in height even at the highest magnifications available in an optical microscope.

Any ordinary metallurgical microscope can be adapted for use with the profile. The set-up is shown in Fig. 1 below. The illuminating system (L_1 and L_2) has a field iris S_2 which focusses onto the surface at X. A fine wire, or series of parallel wires, or a scratch on a disc of glass is mounted close to S_2. The conventional glass illuminater is replaced by a metal tongue T. Thus off-axis illumination is is produced and so the image of the profile wire will appear to have different lateral displacements as the surface height varies. Monochromatic light is used, since the tongue introduces chromatism into the objective optics. An example of a surface profile taken on a bearing surface at X1000. is shown in Fig. 2.

This technique overcomes the snags in the Schmaltz method. Most of the objective aperture is used, all the surface can be seen at the same time as the profile is used, more than one profile is taken at once, and the nature of the image (dark on a bright background) means that scattering effects are not serious. There are no restrictions on the magnifications employed other than those inherent in every microscope. The magnification in depth is given by

$$M' = M \tan i / \mu$$

where M is the lateral manification, i is the angle of incidence of the illuminating light, and μ the immersion refractive index. In practice, the ratio M'/M is found

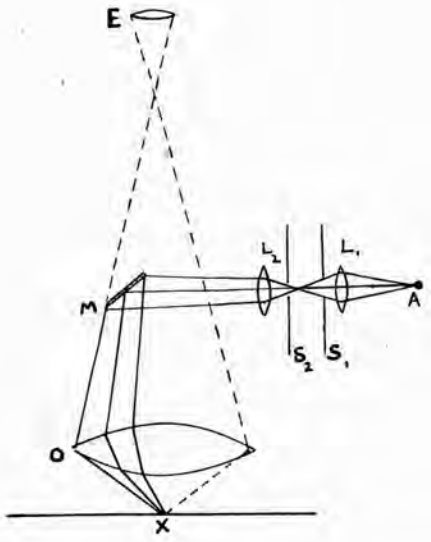

Fig. 1.

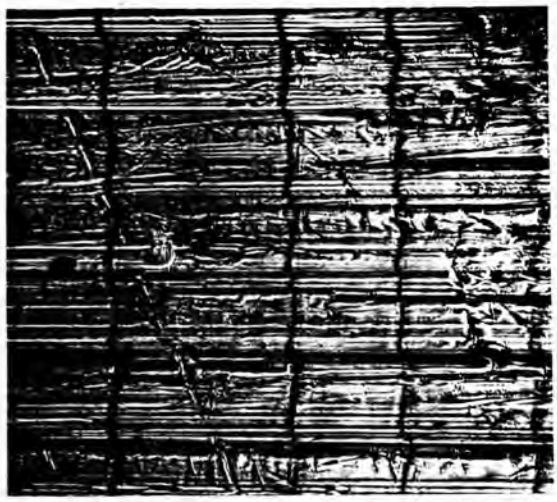

Fig. 2.

experimentally using a depth graticule previously calibrated by F.E.C.O. The table below gives the values of H^1/H found for three objectives used in this laboratory (it is included to give a rough idea of the ratios met with in practise.

Lens	H^1/H
2 mm apo.	1.00
4 mm achro.	1.23
8 mm achro.	0.56

It is interesting that the 2 mm. lens has a ratio H^1 to H of 1.00. The lower powers, which have to be used on the coarser structures due to the finite depth of focus, have lower H/H^1 values.

To sum up, the light profile is a simple and accurate technique, which gives a method, complementary to multiple beam fringes, of measuring surface features down to in height at magnifications up to X 2000, the surface being in full view at the same time. It has been found to be of great value to many workers in the laboratory.

The Optical Shadow Casting Technique.

This is a method of microscopy which is analagous to the metallic shadow casting technique used in electron microscopy for the enhancement of contrast and surface height measurement. Likewise it shows up surface features clearly, and can be employed for measurements of vertical displacements under suitable conditions. The idea (see TOLANSKY, 1953) is that the specimen is illuminated at an angle of incidence near grazing with a small bright pencil of parallel light. The difference between this and darkground illumination is that the light falls onto a special small-grain scattering surface - which may be either a coated slide, upon which the specimen rests, or, as in the case of crystal studies, the specimen itself is coated. The shadows formed by surface features are then clearly visible in the microscope. Provided their height is greater than the wavelength of the light employed, sharp shadows, free from diffraction will be seen, enabling height measurements to be carried out. The magnification is done using approximately spherical particles, e.g. lycopodium powder; either their diameter is found by an alternative method or the ratio of shadow length to width is measured. This calibration, unlike that in the profile method, is independent of the objective in use. The specimen can be explored for the best contrast conditions by riasing and lowering the source and by rotating it about the microscope axis Polarizing the incident beam generally improves the picture.

The scattering surface found to give best results is obtained by evaporating a thick silver layer onto the specimen and holding it over aquaregia until it appears matt white. This

gives an uniform, fine grain scattering surface. The figure below shows this method being used to measure the depth of a trigon on a diamond growth face. The ratio of vertical to lateral magnifications is X12 and the microscope magnification is X 250 so the total vertical mgnification is X2500.

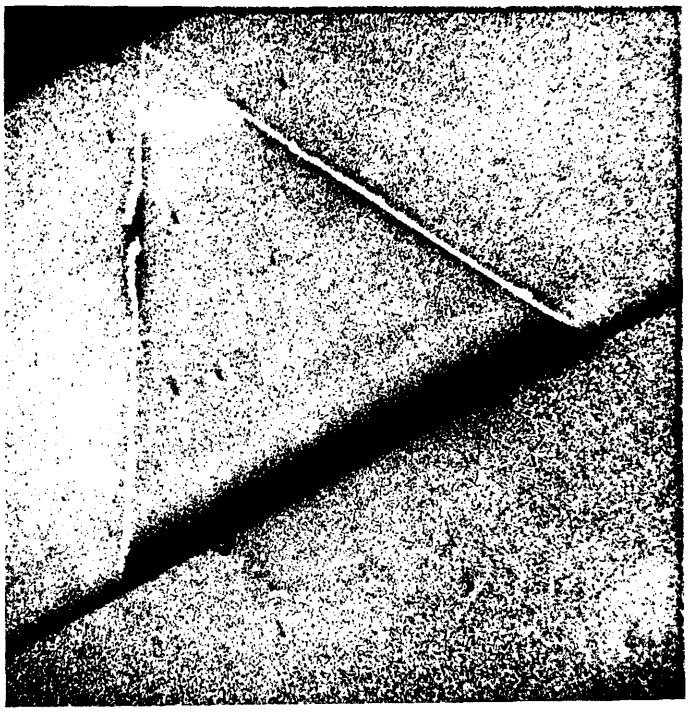

Fig. 3.

Another interesting feature of this technique is shown in this photograph, namely, that the non-horizontal faces facing the beam have enhanced brightness. To sum up, the optical shadow-casting method provides a simple method for revealing and measuring surface structures rather coaser than those which may be tackled by the previous techniques dicussed in part A.

PART B

METHODS WHICH GIVE QUALITATIVE INFORMATION ABOUT THE SURFACE

Phase-Contrast Microscopy.

Soon after the war it was realized that phase microscopy, which up to then had only beenused to observe biological specimens of low amplitude contrast, could be easily applied to the mettaluggical microscope. The early work was done by, JUPNIK, OSTERBERG, and PRIDE, 1946, 1948, and by CUCKOW, 1947, 1949. Later, in 1949, TAYLOR the phase contrast equipment produced by Messers Cooke, Troughton and Simms, which is used extensively in this country.

The theory of phase contrast microscopy has been given in an elementary fom by BENNET et al., 1951, and from a vector point of voew by BARER,1951. As the method has been very adequately described there, it is not desribed here. RICHARDS, 1954, has published a bibliography of phase microscipy which is intended to be ab supplement to the book by Bennet etal. This useful article contains about 200 references.

In biological and medical work the phase contrast features are produced by differences in refractive index ina film of constant thickness, but in reflection metallographic phase contrsat the differences in optical path are produced by changes in metrical distance. See fig. 1 .

WAVEFRONT DISTORTION PRODUCED BY :-

CHANGE IN μ

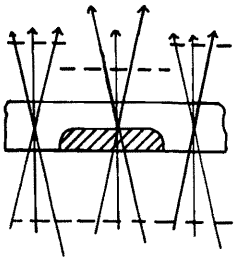

CHANGE IN t

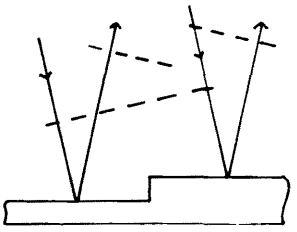

A reflection set-up has been described by TAYLOR,1949 In this, see fig. 2, the light from a high intensity lamp 1, is converged onto the projector annulus,3; An image of this annulus is formed, just above the focal plane of the objective, by the projector lens 4 and the objective 5, at 6. Thus an image of the projector annulus is produced by the surface of the specimen just below its surface, at 7. This it turn is imaged in the plane of the phase plate 8, which is situated ABOVE the beam splitter. The phase plate is above the back focal plane of 6 in the set-up. This isto avoid placing it below the beam splitter, which would give pise to spurous images reflected from the rhase plate. That such an arrangement will give a phase-contrast effect has been shown by OSTERBERG, 1948, who showed that any one of the conjugate pupils which follows the entrance pupil can serve as a location of a phase plate. In the C.T.S. apparatus the phase plates are incorporated in the objective mount, along with the beam splitter. All the various phase plates corresponding

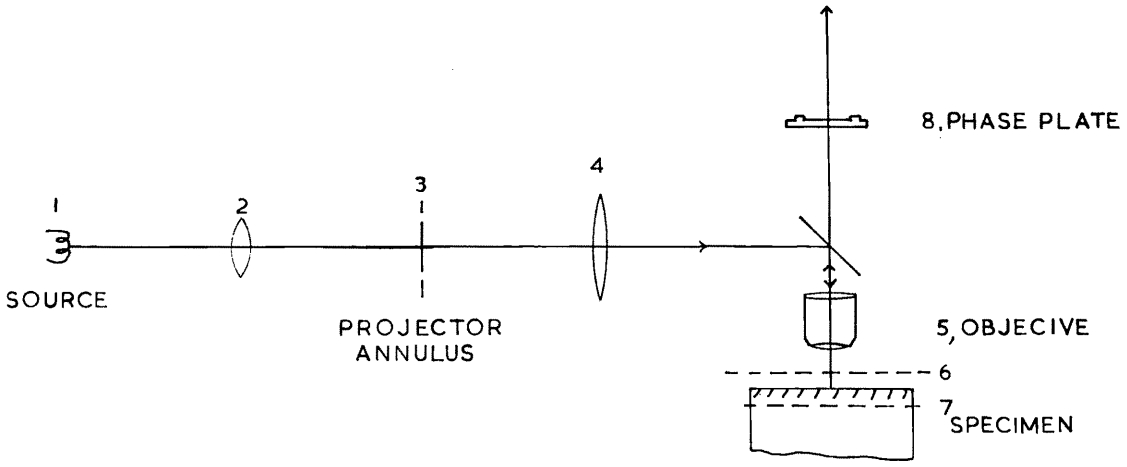
8, PHASE PLATE
4
3
1
2
SOURCE
PROJECTOR
ANNULUS
5, OBJECIVE
6
7
SPECIMEN

to the different objectives have a common ratio of inner and outer diameters corresponding to that of the projector annulus; thus by varing the position of the latter we aan have perfect match between the phase plates and the image of the annulus,3. In reflection phase microscopy the specimens are generally silvered in improve the light situation. The Bauch and Lomb and the Reichart metallographic microscopes are described by BENFORD & SEIDENBERG, 1950, and by GABLER, L953 ,respectively.

The reflection phase contrast technique is very useful in conjunction with multiple beam interference to give an overall picture of the surface. A good example of this is shown in fig.3 below.The plate shows a growth spiral of SiC taken in a) phase contrast and b) reflection Fizeau fringes. Unfortunately, the method can only be used with nearly plane surfaces. Otherwise the various facets of a surface will produce a numser ofsmall images of the projector annulus in ramdome relative positions, which would only result in a highly confused picture, Secondly, the contrast in the image is produced by diffration, which only occurs at abrupt discontiuities in the wavefronts. So little is known about regions where the surface height is varing slowly Furthermore, the halation effect, where a dark image is accompanied by a bright edge and vice-versa, confuses the picture and can lead to false detail, (this is sometimes useful in showing up steps though). Lastly, the phase microscope cannot be used to measure surface features at all (though see FORTY ,L952), although it can detect features only 30 A. high. Like Fizeauu fringes, it has an upper limit too, though it is rather less, being about for normal phase plates.

Fizeau Fringes

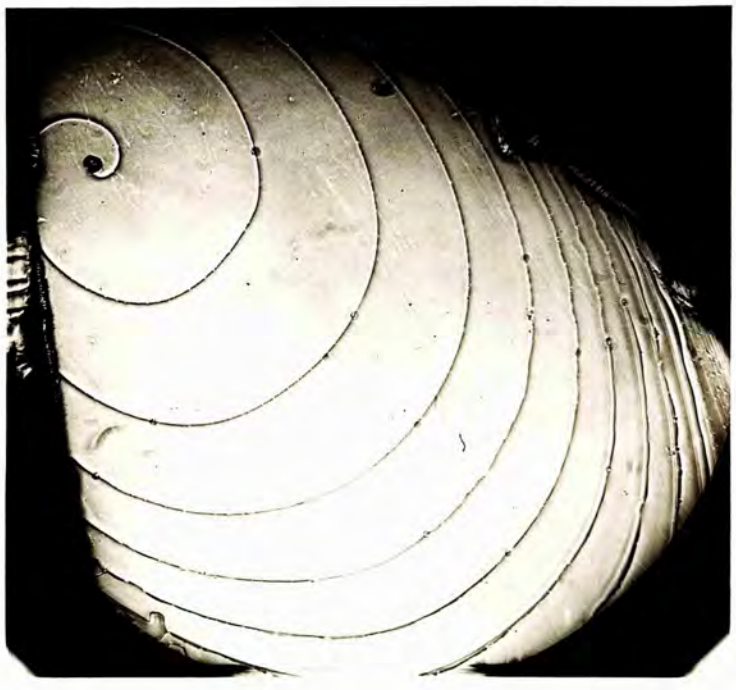

Phase Contrast
Silicon Carbide Growth Spiral

REFERENCES.

Airy, Math. Tracts, 381, (1831).

Banning, J.O.S.A., 37, 792,(1947).

Barer, Series of papers commencing :- J. R. Mic. Soc., 72,10 (1952).

Barr & Jenkins, J.O.S.A., 46, 141, (1956).

Barrell & Teasdale-Buckell, Proc.Phys.Soc, 64, 413, (1951).

Baumeister & Stone, J.OS.A,, 46, 228, (1956).

Belk, PhD. Thesis, London, 1954.

Belk,Tolansky,&Turnbull, J.O.S.A., 44, 5, (1954).

Benford & Seidenburg, J.O.S.A., 40, 259, (1950).

Bennett et al., "Phase Microscopy", Chapman & Hall, 1951.

Bright, Jackson & Kuhn, Proc. Phys. Soc., 62, 225, (1949).

Boulouch, J. de Phys., 2,316, (1893).

Cabrera, C.R.Acad. Sci., 218, 994, (1944).

Crawford, Gray, Schawlow, & Kelly, J.O.S.A., 39. 888, (1949).

Cuckow, Nature, 159, 639, (1947).

" J.Iron & Steel Inst., 161(1), 10, (1949).

Dufour & Pica, Rev. Opt., 24, 19, (1945).

Dufour, Ann Phys., (12,6), 5, (1951).

Dyson, Proc. Roy. Soc., 204, 170, (1950).

"" " " " 216, 493, (1953).

Delayney, Rev. Opt., 32, 610, (1953).

Essig & Holmes, J.O.S.A., 44, 253, (1954).

Fabry, Rev. Opt. 1, 445, (1922).
Fabry & Perot, Ann. de Chem. et de Phys., 12, 459, (1897).
Faust, Phil. Mag., 41, 1238, (1950).
Faust, PhD. Thesis, Manchester, 1949,
Feussner, Gehrche's Handb. der Phys. Opt., Vol (i), (1927).
Forty, Phil. Mag., 43, 949, (1952).

Goos, Z. Phys., 100, 95, (1936).
" " , 106, 606, (1937).

Hamy, J. Phys. Rad., 5, 759, (1906).
Heavens, Optical Properties of Thin Films, Butterworth,(1954).
Holden, Proc. Phys. Soc., 62, 405, (1947).

Jarrett, Nature, 169, 790 , (1952a).
" " , 170, 455, (1952b).
Japnuk, Osterberg, & Pride, J.O.S.A., 710, (1946).
" " " " ,38, 338, (1948).

Kimmel, Z. Angew. Phys., 7, 294, (1955).
Koehler, J.O.S.A., 43, 738, (1953).
Krautkramer, Ann. der Phys., 32, 537, (1938).
Krug & Laue, Technich Berlin, 6,122, (1951).
Kuhn & Wilson, Prog Roy. Soc., 62, 745, (1950).

Laurent, J. Phys., (2), 2, 241, (1883).
Lewis, Thin Films and Surfaces, (1946).
Linnik, C.R.Acad. Sci., U.R.S.S., 21, (193).

MacLaurin, Proc. Roy. Soc., 78, 206, (1906).
Mykura, Proc. Phys. Soc., 67, 201, (1954).

Osterberg, J.O.S.A., 38, 668, (1948).

Penselin & Stendel, Z. Phys., 142, No.i, (1955).
Perry, Research, 8, 255, (1955).
Polster, J.O.S.A., 42, 21, (1952).

Reichert, Microscopy, 7, 43, (1952).
Richards, Science, 120, 631, (1954).
Ring & Wilcock, Nature, 171, 648, (1953).
Rood, J.O.S.A., 39, 854, (1949).
" " , 41, 201, (1951).

Saunders, J. Res. Nat. Bur. Stand., 47, 148, (1951).
Schmaltz, Techn. Oberflachenkunde, 1936.
Schulz, J.O.S.A., 40, 802, (1950).
Sennett & Scott, J.O.S.A., 40, 203, (1950).
Siegbahn, Ark, Mat. Ast. Phys., 23, No. 12, (1933).
Stone, J.O.S.A., 43, 927, (1953).
Strong, Modern Phys. Lab. Practise, 1946).
Strong, J.O.S.A., 30, 431, (1940).

Taylor, J.R.Mic. Soc., 69, 49, (1949).
Tolansky, Phil Mag., 35, 120, (1944a).
" Nature, 153, 195, (1944b).
" " " 314, (1944c).
" " " 435, (1944c).
" Proc. Roy Soc., 184, 41, (1945a).
" " " " " 51, (1945b).

Tolansky, Phil, Mag., 36, 225, (1945c).
" " " 236, (1945d).
Proc. Phys. Soc., 58, 654, (1946c).
Phil. Mag., 37, 390, (1946a).
, 37, 453, (1946b).
High Resolution Spectroscopy, Methuen, 1947.
Multiple Beam Interferometry, O.U.P., 1948.
Vacuum, 2, 231,(1952a).
Z. f Electrochemie, 56, (1952b).
Nature, 169, 445, (1952c).
Lab Practice, p.193, (1952d).
Nature, 171, 564, (1953).
Tolansky & Emara, J.O.S.A., 45, 792, (1954).
Tolansky, Turnbull, & Belk, Lab Practice, L, 403, (1952).

von Cittart, Z. Phys, 65, 547, (1930).

Wilcock, PhD. Theseis, Manchester,L951.

ACKNOWLEDGEMENTS

I wish to express my thanks to Professor S. Tolansky, F.R.S. for interest, advice and encouragement throughout the course of this work. Thanks are also due to my colleagues for much stimulating discussion, particularly Dr V.G. Bhide, and Mrs. V. Hinton, who also kindly lent me many plates as examples to be included in the work. I am much in debt to the Council of the Royal Holloway College for awarding me a Research Studentship in Physics, and I should like to sincerely thank my parents for financial help during my first year here.